Mon. Not. R. Astron. Soc. **000**, 1–16 (2014) Printed 10 February 2015 (MN LATEX style file v2.2)

An early phase of environmental effects on galaxy properties unveiled by near-infrared spectroscopy of protocluster galaxies at z > 2

Rhythm Shimakawa[1,2⋆], Tadayuki Kodama[2,3⋆], Ken-ichi Tadaki[3,4], Masao Hayashi[3], Yusei Koyama[3,5], and Ichi Tanaka[1]

[1] *Subaru Telescope, National Astronomical Observatory of Japan, 650 North A'ohoku Place, Hilo, HI 96720, USA*
[2] *Department of Astronomy, School of Science, Graduate University for Advanced Studies, Mitaka, Tokyo 181-8588, Japan*
[3] *Optical and Infrared Astronomy Division, National Astronomical Observatory, Mitaka, Tokyo 181-8588, Japan*
[4] *Max-Planck-Institut für Extraterrestrische Physik, Giessenbachstrasse, D-85748 Garching, Germany*
[5] *Institute of Space Astronomical Science, Japan Aerospace Exploration Agency, Sagamihara, Kanagawa, 252-5210, Japan*

arXiv:1406.5219v3 [astro-ph.GA] 7 Feb 2015

Re-submitted 2014 November 25. Version 2.

ABSTRACT

This work presents the results from our near-infrared spectroscopy of narrow-band selected Hα emitters (HAEs) in two rich overdensities (PKS 1138–262 at z=2.2 and USS 1558–003 at $z = 2.5$) with the Multi-Object Infrared Camera and Spectrograph (MOIRCS) on the Subaru telescope. These protoclusters are promising candidates for the most massive class of galaxy clusters seen today (Paper I). The confirmed HAEs in the protoclusters at $z > 2$ show high excitation levels as characterized by much higher [OIII]/ Hβ or [OIII]/ Hα line ratios than those of general galaxies at low-z. Such a high excitation level may not only be driven by high specific star formation rates (sSFRs) and lower gaseous metallicities, but also be contributed by some other effects. We investigate the environmental dependence of gaseous metallicities by comparing the HAEs in the protoclustrers with those in the general field at similar redshifts. We find that the gaseous metallicities of protocluster galaxies are more chemically enriched than those of field galaxies at a given stellar mass in the range of $M_\star \lesssim 10^{11}$ $M_\odot$. This can be attributed to many processes, such as intrinsic (or nature) effects, external (or nurture) effects, and/or some systematic sampling effects. The intrinsic (nature) effect leads to the advanced stage of 'down-sizing' galaxy evolution in protoclusters. On the other hand, the external (nurture) effects include the recycling of chemically enriched gas due to the higher pressure of intergalactic medium and/or stripping of outer gas in the reservoir in protoclusters. We also find that the offset of the mass–metallicity relation in dense environment becomes larger at higher redshifts. This can be naturally understood by the fact that the inflow/outflow rates in star-forming galaxies are much higher at higher redshifts. Therefore, the environmental dependence of such 'feeding' and 'feedback' mechanisms in galaxy formation is probably playing major roles in producing the offset of the mass–metallicity relation for the protocluster galaxies at $z > 2$.

Key words: galaxies: clusters: general — galaxies: evolution — galaxies: formation

1 INTRODUCTION

Local galaxy clusters ($z < 1$) are dominated by red spheroidal galaxies and exhibit well-known relations, such as the colour–magnitude relation (red sequence) and morphology–density relation (Butcher & Oemler 1984; Dressler et al. 1994, 1997; Kodama & Bower 2001). The environmental dependence of such galaxy properties in the local Universe seems to originate from two effects, 'nature' and 'nurture'. The nature effect means that galaxies formed in dense environments are more evolved intrinsically due to biased galaxy formation, and thus are older hence redder (Bower, Kodama & Terlevich 1998; Thomas et al. 2005). In contrast, the nurture effect means that today's early-type galaxies in dense regions have been deformed through external effects from the surrounding

⋆ E-mail: rhythm@naoj.org (RS); t.kodama@nao.ac.jp (TK)

environments (Okamoto & Nagashima 2003; Prieto et al. 2013). For instance, galaxy mergers are expected to occur more frequently in high-redshift galaxy (proto-)clusters (Gottlöber, Klypin & Kravtsov 2001). In fact, dispersion dominated early-type galaxies are common in clusters (as reported by large kinematic studies such as ATLAS3D; Cappellari et al. 2011). These may have formed via a major merger, which can produce a compact spheroidal galaxy through a dissipational kinematical process as predicted theoretically by many authors (e.g. Mihos & Hernquist 1996; Bournaud, Jog & Combes 2007; Hopkins et al. 2008).

In order to identify the physical processes that are responsible for the establishment of the environmental dependence, we need to trace back the history of galaxy formation and evolution in clusters. "Protoclusters" at $z \gg 1$ are the ideal laboratories to investigate the progenitors of massive early-type galaxies in present-day rich clusters. Kodama et al. (2007) showed that the tight red sequence at the bright end of luminosities breaks down in protoclusters in the redshift interval of $2 < z < 3$, which suggests that this epoch is a transition period of cluster galaxy formation. It is therefore essential to systematically explore properties of star-forming (SF) galaxies in protoclusters at $2 < z < 3$ in order to understand how the environmental dependence is established.

With this motivation, several works have been devoted to the investigations of the environmental dependence of SF in protoclusters. In particular, Kodama et al. (2013) conducted a systematic study of protoclusters at $z > 1.5$ with Subaru, as part of the 'Mahalo-Subaru' (*Mapping HAlpha and Lines of Oxygen with Subaru*). The Mahalo project targets 8 known clusters/protoclusters at $1.4 < z < 2.6$, and an un-biased field SXDS-UDS-CANDELS for comparison ($z = 2.19$ and 2.53 slices). We employ narrow-band (NB) filters on the two wide-field cameras, Subaru Prime Focus Camera (Suprime-Cam) and the Multi-Object Infrared Camera and Spectrograph (MOIRCS) on the Subaru telescope. Many NB filters are manufactured for the purpose of identifying Hα or [OII] emitter candidates at that are physically associated with the clusters/protoclusters, as well as those located in narrow redshift slices in the field for comparison. The advantage of using the NB technique is that we can make a SFR limited sample with a high completeness, and the selection bias is minimized due to homogeneous, well-defined sampling using the star formation indicators.

It has been shown that the SF activity is high even in the cores of protoclusters at $z > 2$, which scales as $(1 + z)^6$ (Shimakawa et al. 2014b), or more rapidly (Smail et al. 2014; Shapley et al. 2005b). The peak of SF activity traced by line emitters is shifted from dense cluster cores to lower density outskirts and filamentary outer structures with time from $z \sim 2.5$ to $z \sim 0.4$, indicating the inside-out growth of clusters (e.g. Hayashi et al. 2012; Koyama et al. 2013a; Hayashi et al. 2011; Koyama et al. 2010; Kodama et al. 2004 in the order of decreasing redshift from 2.5 to 0.4).

During such a turbulent, active epoch for galaxy formation, the physical conditions of inter-stellar medium (ISM) are expected to change. However, physical properties of line emitters in the protoclusters remain unclear so far. In the case of SF galaxies in general fields, for example, they form a tight sequence on the Baldwin, Phillips and Terlevich (BPT) diagram (Baldwin, Phillips & Terlevich 1981; Veilleux & Osterbrock 1987) known as the *(chemical-)abundance sequence* (Dopita et al. 2000; Kauffmann et al. 2003) and we can see more extremely ISM conditions at high-z on this diagram as noted by many authors (Shapley et al. 2005a; Erb et al. 2006a; Yabe et al. 2012; Newman et al. 2014; Kewley et al. 2013b,a; Nakajima et al. 2013; Yabe et al. 2014b; Masters et al. 2014; Steidel et al. 2014; Shapley et al. 2014; Coil et al. 2014). The abundance sequence of SF galaxies is shifted upward and/or rightward at high redshift (towards higher [OIII]/Hβ or [NII]/Hα line ratios), and such a tendency is also seen in the field population at $z > 2$ (Erb et al. 2006a; Newman et al. 2014; Kewley et al. 2013b; Masters et al. 2014).

In local galaxies, the ISM conditions are often described by some physical quantities such as ionization parameter (q), gaseous metallicity (Z) and electron density (n_e). At high-redshift, the ionization parameter is raised by a large flux of ionizing photons in ISM originated from hot O, B stars due to intensive star formation in relatively small galaxies. Previous studies suggest a high ionization parameter of SF galaxies at $z > 2$ compared to that of local galaxies (Erb et al. 2010; Nakajima et al. 2013; Nakajima & Ouchi 2014; Masters et al. 2014). Secondly, the chemical abundances of SF galaxies at $z \sim 2$ is lower by 0.1–0.3 dex for a given stellar-mass compared to those at low-z (Erb et al. 2006a; Steidel et al. 2014; Sanders et al. 2014). This leads to more compact and hotter O, B stars due to lower opacity (Ezer & Cameron 1971; Maeder 1987), and thus UV radiation becomes harder and produces more ionizing photons. Thirdly, the strength of collisionally-excited emission lines (e.g. [OIII], [NII]) strongly depends on the electron density. It is closely related to the number of electrons to collide since the excitation potential of this line is $\sim$1eV, which is nearly the same as the energy of electrons at the virial temperature ($\sim 10^4$ K) (Dyson & Williams 1980). Due to low excitation potential, the transition of collisionally-excited line is reliant on electron density compared to gaseous metallicity. Recent observations have suggested a high electron density ($n_e > 100$ cm^{-3}) in SF galaxies at $z \sim 2$ (Newman et al. 2012; Masters et al. 2014; Shirazi, Brinchmann & Rahmati 2014; Wuyts et al. 2014). This value is larger than that of normal SF galaxies at low-z by an order of magnitude, and close to that of interacting galaxies which are seen as (ultra) luminous infrared galaxies (ULIRGs/LIRGs) in the present-day Universe (Krabbe et al. 2014). Such a large electron density contributes to the offset of galaxy distributions on the BPT diagram together with other physical parameters (Brinchmann, Pettini & Charlot 2008). In this way, the cosmic dependence of the BPT diagram can be attributed to such physical parameters which determine ISM conditions.

An obvious extension of such studies is to investigate the environmental dependence of the ISM properties at $z > 2$ to test whether the evolutionary stages of SF galaxies, such as their chemical abundance, are environmentally dependent. Protocluster galaxies may go through active nuclear starbursts followed by a quiescent phase due to higher chance of galaxy-galaxy mergers (Gottlöber, Klypin & Kravtsov 2001). Such nuclear starbursts would cause higher electron densities and harder UV radiation of the ISM (Shimakawa et al. 2014a), which lead to different gas excitation in the dense environments.

Furthermore, we also want to address the environmental dependence of some characteristic relations of SF galaxies such as the mass–metallicity (M–Z) relation (Tremonti et al. 2004; Kewley & Ellison 2008; Maiolino et al. 2008; Yabe et al. 2012; Zahid et al. 2013), since this relation reflects the star formation histories, as well as inflow/outflow processes in galaxies (Erb et al. 2006a; Erb 2008; Zahid et al. 2014a; Yabe et al. 2014a). For example, if protocluster galaxies formed at the earliest times (Thomas et al. 2005), the M–Z relation in the dense environments might be explained to be more evolved (i.e., offset to higher metallicity) compared to that in lower density regions at the same redshift.

In this paper, we aim to explore the gaseous physical properties and its environmental dependence using near-infrared (NIR) spectroscopy of SF galaxies in two well studied protoclusters from the MAHALO-Subaru sample, namely PKS 1138–262 at $z = 2.16$ (Koyama et al. 2013a) and USS 1558–003 at $z = 2.53$ (Hayashi et al. 2012), which are among the richest systems so far identified at $z > 2$ (Shimakawa et al. 2014b). Since they both show large excesses in the number density of SF galaxies, these protoclusters are still in the vigorous formation process of present galaxy clusters.

At the redshift interval of $1.5 < z < 2.5$, many important strong emission lines, including Hα, which are well-calibrated in local galaxies in the rest-frame optical, are all redshifted to the NIR regime (λ=1.0–2.3 μm). Our targets are selected from the NB (Koyama et al. 2013a; Hayashi et al. 2012), and thus NIR spectroscopy is efficient since the Hα emission is detectable at high signal-to-noise ratio (S/N) in a few hours.

From the NIR spectroscopy, we investigate the following quantities of our Hα selected SF galaxies at $z > 2$. We will measure the strength of dust attenuation using the Balmer decrement technique (Hα/ Hβ line ratios) and such as. We will study gaseous metallicities using the Pettini & Pagel (2004) prescription (N2 index), excitation states, and the contribution (or contamination) of active galactic nucleus (AGN) using [NII]/ Hα versus [OIII]/ Hβ diagram (BPT) (Veilleux & Osterbrock 1987) and stellar-mass versus [OIII]/ Hβ diagram (MEx) (Juneau et al. 2011). We then investigate the environmental dependence of the M–Z relation.

We first describe our data and the analyses. We then show our results from various aspects; dust extinction (§3.1), MEx diagram (§3.2), BPT diagram (§3.3), and M–Z relation (§3.4). We discuss the differences of the physical properties and the SF activities between low versus high redshifts, and field versus dense environments. The final section gives the conclusions of this work.

This work assumes the cosmological parameters of Ω_M=0.3, Ω_Λ=0.7 and H_0=70 km/s/Mpc. We employ the Salpeter (1955) initial mass function (IMF). When we show the results in the literature that use the Chabrier (2003) IMF, we scale up SFRs and stellar masses by a factor of 1.8 to match them to the case of the Salpeter IMF.

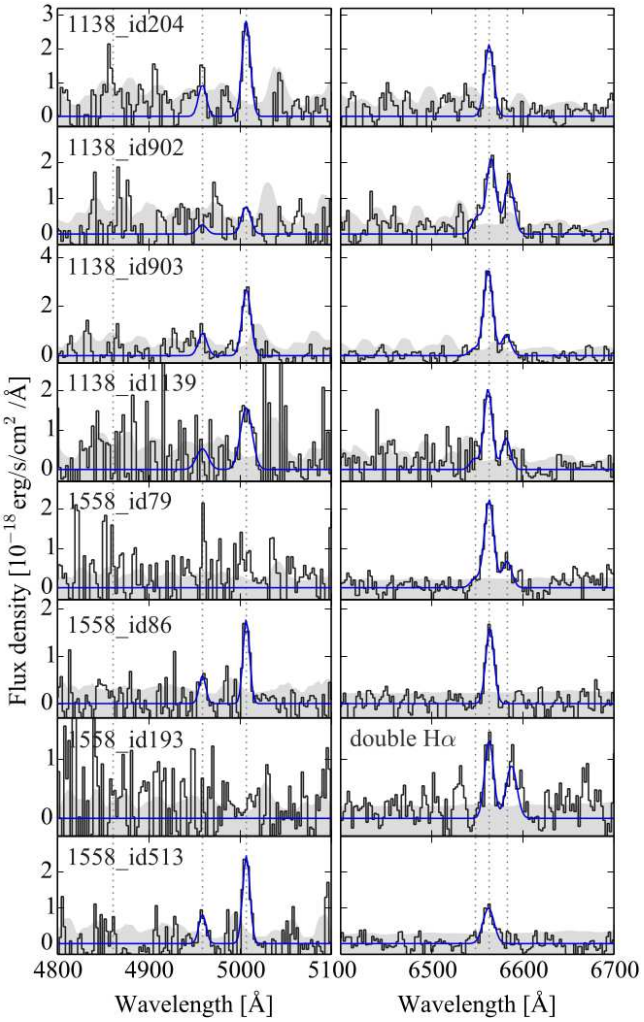

Figure 1. Examples of the spectra of HAEs in the PKS1138 and USS1558 protoclusters. The black, blue line and grey filled region show reduced spectra, fitting curve, and sky Poisson noise levels. We here subtract a continuum of each spectrum. The dotted vertical lines show [NII]6583Å Hα6563Å [NII]6548Å [OIII]5007Å [OIII]4959Å Hβ4861Å emission lines from the right side.

2 DATA & ANALYSIS

2.1 Observational data

In this paper, we study the physical properties of HAEs in the two protoclusters associated with radio galaxies, PKS 1138–262 ($z = 2.16$; hereafter PKS1138) and USS 1558–003 ($z = 2.53$; hereafter USS1558). In the respective protoclusters, 48 and 68 HAE candidates that show excesses of NB fluxes above 3σ threshold and are also identified as cluster memberships from a broad-band colour-colour diagram ($Bz'K_s$ or $r'JK_s$) to separate Hα emitters (HAEs) at the cluster redshift from contaminant [OIII]/ [OII]/ Paα emitters at other redshifts (see Koyama et al. 2013a; Hayashi et al. 2012 for more details).

The spectroscopic observations of these candidates were conducted in 2013 April with MOIRCS, a NIR imager and spectrograph (Ichikawa et al. 2006; Suzuki et al. 2008) mounted on the 8.2-m *Subaru* telescope on Mauna Kea. We employed 3 slit masks for each protocluster, and a typical

slit mask includes about 20 science targets. The net integration time was 2 to 3 h per mask, and the typical seeing size was about 0.7 arcsec. In total 98 HAE candidates were observed by using the low resolution grism (HK500: λ=1.3–2.5 μm, $R\sim$500 for 0.8 arcsec slit width) for 5 masks, and the high-resolution grism (VPH-K: λ=1.9–2.3 μm, $R\sim$1700 for 0.8 arcsec slit width; see Ebizuka et al. 2011) for one of the three masks of PKS1138. A summary is given in Table 1 (see also Shimakawa et al. 2014b).

We reduced the obtained spectra using the MOIRCS MOS Data Pipeline (MCSMDP: Yoshikawa et al. 2010) that is an IRAF based data reduction software for spectroscopic data of MOIRCS [1]. This reduction package was designed to operate standard procedures semi-automatically which consists of bad pixel masking, cosmic rays filtering, A−B subtraction, wavelength calibration, distortion correction, and background subtraction (more detail is described in Yoshikawa et al. 2010). Then, we conducted a flux calibration based on a standard star with a A0V spectrum and the K-band magnitude of 9.930. Reduced spectra show the mean 1σ sky noise of m_{AB}=22.2–22.6 and the root-mean-square error (rms) of wavelength calibration of about Δv=±40–50 km/s. Firstly, we looked for Hα emission lines at around the protocluster redshifts within ±2000 km/s, and performed a Gaussian fitting using the software SPECFIT (Kriss 1994) distributed within STSDAS[2] layered on top of the IRAF environment. We usually used a single Gaussian fitting iteratively, but sometimes applied a multi-Gaussian fitting for a broad or a multiple blended emission line, and then the chi-square minimization technique was used to best fit the line profile. We here included sky Poisson noises, $\sigma(\lambda)$, as a parameter in the line fitting. The 1σ flux errors discussed throughout this paper were produced by this process, and hence they include both fitting errors and sky noise.

We identify Hα emission lines at above 3σ levels for 28 and 37 emitters in PKS 1138 and USS 1558 protoclusters, respectively. However, each one of them have been identified as background [OIII] emitter since it has doublet lines [OIII]λ4959/5007 in each protocluster region. Also, we could not find any objects which have emission lines only outside the wavelength of the response curves of the NB filters. The remaining 37 non-detections tend to have lower NB fluxes or larger stellar masses, which indicates that our spectroscopy is not sensitive enough to detect faint or broad emission lines.

This work adopts confirmed HAEs detected by the low resolution grism (Table 1), since we can discuss the physical properties inclusive of [OIII] and Hβ lines. Therefore, final sample is composed of 24 and 36 HAEs in PKS 1138 and USS 1558, respectively. While about a half of the resultant spectra show [OIII] lines coupled with Hα lines with above 3 sigma level, [NII] and Hβ lines cannot be detected in most of the sample. Some examples of the resultant spectra including best fit curves, and sky Poisson noise levels are shown in Fig. 1.

In this work, we often use the NB flux, stellar-mass, and optical band magnitude derived from the previous imaging surveys with MOIRCS and Suprime-cam (Koyama et al. 2013a; Hayashi et al. 2012). For comparison of our data with field counterparts at the similar redshifts, we are referring several samples as reported by Newman et al. (2014); Erb et al. (2006a) These data sets are based on UV colour (Adelberger et al. 2004). This may cause significant descrepancies from our Hα-selected sample. We discuss the effects of sampling bias in the section 4.2. Also, we use SDSS sample (Abazajian et al. 2009) at $0.04 < z < 0.3$ as comparison of the galaxies at between low redshift and high redshift, and we cite their stellar masses and SFRs from Kauffmann et al. (2003); Salim et al. (2007) and Brinchmann et al. (2004), respectively. All of those IMF are corrected to the Salpeter (1955) IMF. Through this paper, we select the SDSS galaxies with equivalent width (EW) of Hα emission line greater than 20Å, because our data are based on the previous NB imaging (Koyama et al. 2013a; Hayashi et al. 2012) which selects the HAEs with $\mathrm{EW_{H\alpha}}$ >20Å in the rest frame. Moreover, we select only those whose [NII]λ6583Å, H$\alpha\lambda$6563Å, [OIII]λ5007Å and H$\beta\lambda$4861Å emission lines are all detected more than 3σ reliability.

2.2 Stacking analysis

27 and 36 HAEs in PKS1138 and USS1558 have been confirmed. For 13 and 17 confirmed HAEs in respective protoclusters, we also detect [OIII] lines. As shown in the next section, we study their physical properties on the [OIII]/Hβ line ratio versus stellar-mass plane based on their [OIII]/Hα line ratios by assuming an appropriate dust correction from their UV/Hα luminosity ratios. It is not ideal to discuss the physical properties of the protocluster galaxies with only Hα and [OIII] lines. In most of the individual spectra, however, do not detect [NII] or Hβ emission lines above a S/N=3. In order to study physical properties of protocluster galaxies such as metallicity and excitation and compare them with those of field galaxies at the same redshifts, we need four emission lines (Hα, [OIII], [NII], Hβ).

We thus apply a stacking analysis by summing the individual spectra. This technique is useful to investigate 'average' properties. Here, we stack the individual spectra using the S/N as the weight. We divide our sample into two bins by stellar mass in each protocluster with approximately equal numbers per bin as shown in Table 2 (PKS1138-low, -high and USS1558-low, -high). In the stacking analysis, we only use the spectra taken by the low-resolution grism HK500. The spectral stacking is done using the following equation,

$$F_{stack}(\lambda) = \sum_i^n \frac{F_i(\lambda)}{\sigma_i(\lambda)^2} / \sum_i^n \frac{1}{\sigma_i(\lambda)^2}, \quad (1)$$

where $F_i(\lambda)$ is a flux density of an individual spectrum and $\sigma_i(\lambda)$ is a sky poisson noise as a function of wavelength. We then apply the least chi-square fitting technique to the stacked line profiles by multi Gaussian curves with SPECFIT as we apply to the individual spectra. We sum up the spectra with a 'median' combine, as it produces a spectrum with the highest S/N as it suppresses the sky line residuals.

The spectral fitting results are shown in Fig. 2. We see detections of [NII] and Hβ lines (although at low S/N) in most of the stacked spectra. Also, clear mass dependences of [NII], [OIII], and Balmer lines can be found in the sense

[1] IRAF is distributed by National Optical Astronomy Observatory and available at iraf.noao.edu/

[2] Available at www.stsci.edu/institute/software_hardware/stsdas/

Table 1. A summary of data-sets obtained and used in this work. Columns: (1) protocluster name, (2) redshift, (3) the number of HAE candidates selected by the combined technique of NB and broad-band (Koyama et al. 2013a; Hayashi et al. 2012), (4) 3σ limit of SFRs (without dust correction) of HAEs in the past studies, (5) grism name, (6) spectral resolution with 0.8 arcsec slit width, (7) integration time, (8) the number of science objects in each slit mask, (9) the number of total observed targets by low resolution grism, HK500 (including VPH-K), and (10) the number of confirmed cluster members by HK500 (including VPH-K).

Protocluster (1)	z (2)	HAE (3)	SFR_{lim} (4)	Grism (5)	R (6)	Int. time (7)	Slit (8)	Target (9)	Confirmation (10)
PKS 1138–262	2.156	48	$\sim$10 $M_\odot$/yr	HK500	513	120 min	23	36 (44)	24 (27)
(α_{J2000}, δ_{J2000})				HK500	513	161 min	19		
(175.2013, –26.4858)				VPH-K	1675	225 min	18		
USS 1558–003	2.533	68	$\sim$8 $M_\odot$/yr	HK500	513	180 min	25	54	36
(α_{J2000}, δ_{J2000})				HK500	513	276 min	19		
(240.3221, –0.4797)				HK500	513	175 min	15		

Table 2. Properties of the stacked spectra of Hα emitters in PKS1138 and USS1558 separated into two stellar mass bins (low and high) and the same stellar-mass bin for comparing with each protocluster (mid). (1) ID categorized by stacking method, (2) number of galaxies in each bin, (3) the median stellar-mass, 1σ scatter and (4) stellar-mass range of individual spectra used in stacking.

ID (1)	Num. (2)	$\log(M_\star/M_\odot)$ (3)	$\log(M_\star/M_\odot)$ range (4)
PKS1138-low	13	$9.99^{+0.43}_{-0.73}$	8.60–10.54
PKS1138-high	9	$11.16^{+0.20}_{-0.34}$	10.68–11.56
USS1558-low	15	$9.66^{+0.32}_{-0.48}$	8.98–10.08
USS1558-high	11	$10.64^{+0.19}_{-0.24}$	10.21–11.07
PKS1138-mid	11	$10.15^{+0.22}_{-0.19}$	9.86–10.54
USS1558-mid	7	$10.25^{+0.20}_{-0.23}$	9.83–10.56

that the stacked spectra of high stellar mass bins tend to have stronger [NII] and weaker [OIII] compared to those of lower mass bins (see also Shapley et al. 2014). In addition, for a direct comparison between the two different protoclusters, we also stack the spectra with a common stellar mass bin, and they are represented by PKS1138-mid and USS1558-mid. However, we cannot find any difference between the two observed protoclusters in the stacked spectra of the same stellar-mass bin (Table 2). Therefore we hereafter only show the stacked spectra of PKS1138-low, -high, USS1558-low, and -high, to improve visibility of the figures, unless otherwise noted.

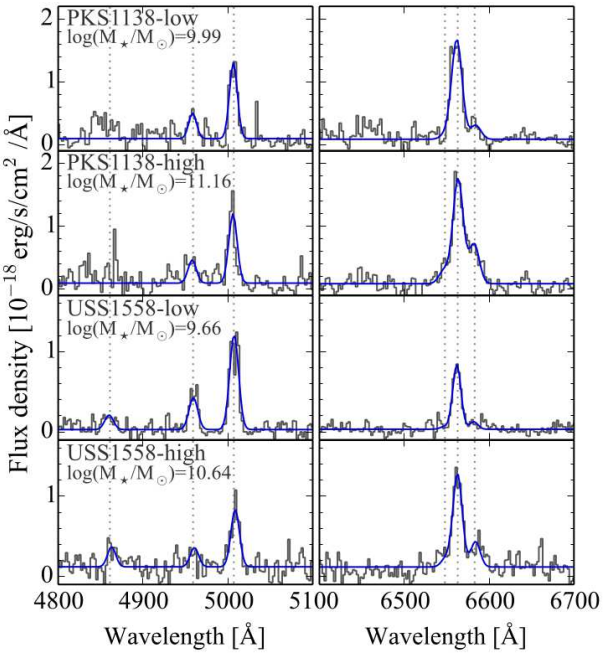

Figure 2. The resultant stacked spectra (from top to bottom: PKS1139-low, -high, USS1558-low, and -high). Grey and blue curves show stacked spectra and the results of the spectral fit. Dotted vertical lines are the same as those in Fig. 1.

3 PHYSICAL STATES OF SF GALAXIES

The physical properties of SF galaxies in dense environments may provide us with information on how those galaxies are formed, and affected by their surrounding environments (such as galaxy-galaxy mergers), and how they evolve together with central supermassive black holes.

3.1 Dust extinction

We here investigate the dust attenuation of the protocluster galaxies at $z > 2$ in two ways, first, based either on the Balmer decrement or second on the ratios between SFR(Hα) and SFR(UV) (Kashino et al. 2013; Wuyts et al. 2013; Koyama et al. 2014) by assuming the Calzetti et al. (2000) extinction curve, $k(\lambda)$.

In the former case, we estimate the amount of dust extinction for Hα flux using the observed Hα/Hβ line ratio measured from the stacked spectra,

$$A_{\mathrm{H}\alpha,\mathrm{Balmer}} = 6.535\ \log(F_{\mathrm{obs}}(\mathrm{H}\alpha)/F_{\mathrm{obs}}(\mathrm{H}\beta)) - 2.982 \quad (2)$$

We here assume that the intrinsic Hα/Hβ line flux ratio is 2.86 for a Case B recombination in the gas temperature of T_e=10^4 K and the electron density of $n_e = 10^2$ cm^{-3} (Brocklehurst 1971).

In the latter case, the extinction magnitude for a Hα line can be estimated by the following equation:

$$A_{\mathrm{H}\alpha,\mathrm{UV}} = A_{\mathrm{UV}} + 2.5\ \log(\mathrm{SFR}_{\mathrm{obs}}(\mathrm{UV})/\mathrm{SFR}_{\mathrm{obs}}(\mathrm{H}\alpha)), \quad (3)$$

where SFR(UV) is estimated by using the Kennicutt (1998) conversion and SFR(UV)=1.4×10^{-28} L_ν erg/s/Hz. We calculate L_ν from the B-[3] and r'- band fluxes ($\lambda_{\rm rest}\sim$1400Å and 1770Å for PKS1138 and USS1558, respectively). According to the Calzetti et al. (2000) prescription for dust extinction, $k(\lambda)$ values at three relevant wavelengths are $k(\lambda6563Å)=k_{\rm H\alpha}=3.33$; $k(\lambda1400Å)=10.78$; $k(\lambda1770Å)=9.48$. The actual absolute values of extinction depend also on the effective obscuration factor, $R_V=A_V/E_s(B-V)$. This work adopts $R_V=4.05$ (Calzetti et al. 2000). SFR$_{\rm obs}$(Hα) is also estimated by the Kennicutt (1998) calibration, SFR$_{\rm obs}$(Hα)=$7.9\times10^{-42}L_{\rm H\alpha}$, where $L_{\rm H\alpha}$ is the Hα line luminosity. We use the Hα flux estimated from the NB flux (F(NB)) to avoid any flux loss. The NB fluxes are sampled by our previous works (Koyama et al. 2013a; Hayashi et al. 2012). It should be noted that F(NB) usually contains [NII] emission line flux, and we need to correct for such contamination. Here we apply a mass-dependent flux correction. The correction is determined as a function of stellar-mass using the correlation between stellar-mass and [NII]/Hα line ratio that we derive from the stacking analysis, which is equivalent to the mass–metallicity relation (sees more detail in §3.4).

Furthermore, we need to convert from stellar absorption to nebular attenuation ($A_{\rm nebula}\propto A_{\rm star}/f$). The strength of dust obscuration depends not only on dust-to-gas ratio but also on the geometry of dust and OB stars in HII regions where the emission lines originate. We explore an appropriate extra extinction of nebular emission lines compared to that of stellar light since it is critical for studying physical properties of SF galaxies as discussed by many authors (Yoshikawa et al. 2010; Kashino et al. 2013; Wuyts et al. 2013; Whitaker et al. 2014). Kashino et al. (2013) have reported that f value can be larger for distant SF galaxies at $z>1$ (f=0.69–0.83) based on $sBzK$-selected galaxies (Daddi et al. 2007). On the other hand, if the cloud scaling relation reported by Larson (1981) breaks down at high redshifts, the proportionality would change (Wuyts et al. 2013). Wuyts et al. (2013) have proposed a new approach for dust correction, which uses a non-linear conversion from stellar to nebular extinctions based on 473 massive SF galaxies ($M_\star>10^{10}$ $M_\odot$) at $0.7<z<1.5$ who derive $A_{\rm nebula}=A_{\rm star}(1.9-0.15A_{\rm star})$.

We investigate an appropriate f value which can give consistent dust attenuation values for HAEs in USS1558 with both the Balmer decrement technique and the UV/Hα method. After trial and error attempts, a linear conversion factor is found to be more favorable for our sample since the Wuyts et al. (2013) prescription shows much higher $A_{\rm H\alpha,UV}$ (0.5–1.0 dex) on average compared to $A_{\rm H\alpha,Balmer}$ of the stacked data. This paper uses the best value of f=0.66. Figure 3 shows $A_{\rm H\alpha}$ versus stellar-mass relation. With the f value and the prescrption as described above, the discrepancy, $\Delta A_{\rm H\alpha}=A_{\rm H\alpha,Balmer}-A_{\rm H\alpha,UV}$ gets as small as -0.021 for HAEs with $M_\star<10^{10.1}M_\odot$ (USS1558-low) and $+0.016$ for those with $M_\star>10^{10.2}M_\odot$ (USS1558-high). From now on, we ignore such small residuals as they have no impact on our results. In Fig. 3, local relationship for the SDSS galaxies is also shown by a dotted curve (Garn & Best 2010). While we do not see any significant difference in Hα extinction of our sample compared to the local sequence, we identify 7 heavily-obscured objects with $A_{\rm H\alpha}>3$ in the protoclusters. In particular, one of them seen in USS1558 that shows a significant excess from other galaxies ($A_{\rm H\alpha}>4$) has a total IR luminosity of $5\times10^{12}L_\odot$ and its radio continuum is detected by the Jansky Very Large Array (Tadaki et al. 2014). More details regarding the dusty and starburst populations and their environmental dependence will be discussed in a forthcoming paper.

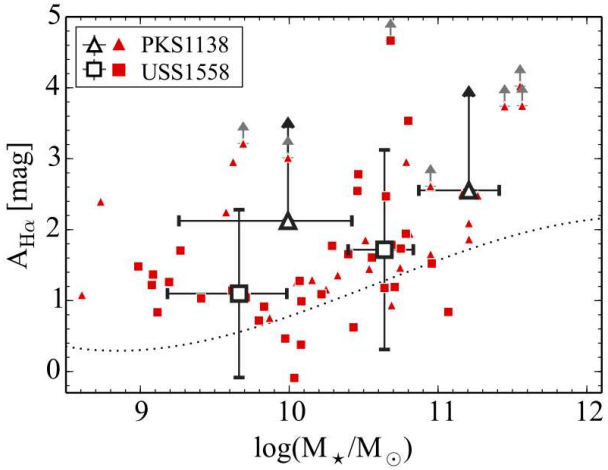

Figure 3. Dust extinction of Hα lines as a function of stellar mass. Large open triangles and squares indicate the stacked spectra of HAEs in PKS1138 and USS1558, respectively, and their error-bars represent $\pm$ 1 σ errors. Red filled triangles and squares show the individual HAEs in PKS1138 and USS1558, respectively. For the objects whose detection significance is lower than 2σ in the B-band, we use the 2σ limiting magnitude in B or r'-band to estimate the UV flux. We also use the 2σ flux if the Hβ flux of a stacked spectrum is less than the 2σ detection limit to estimate $A_{\rm H\alpha,Balmer}$. Dotted curve is an empirical sequence of SDSS galaxies reported by (Garn & Best 2010).

3.2 Mass–excitation diagram

Various line ratios reflect physical properties, such as gaseous metallicity, ionization parameter, and electron density of the ionized gas in HII regions. Line ratios are usually measured for sets of strong lines such as [OIII]/Hβ and [NII]/Hα, located nearby in wavelength so that the ratio is almost free from dust extinction. In order to derive the physical quantities from the line ratios, many authors have improved the line diagnostics using theoretical models and/or the empirical calibrations based on local galaxies. Among them, some traditional treatments are widely used, such as BPT diagram (Baldwin, Phillips & Terlevich 1981, see §3.3) and mass-metallicity relation (Tremonti et al. 2004, see §3.4). In §3.2–3.4, we show the physical properties of HAEs in the protoclusters based on several line diagnostics, and compare them with SDSS local galaxies and the field galaxies at similar redshifts (z=2.1–2.5).

This MOIRCS spectroscopy not only confirms the existence of Hα emission line for a large number of NB-selected

[3] The B-band data of PKS1138 field was originally published by Kurk et al. (2000, 2004)). Source photometry was performed by Koyama et al. (2013a) at the positions of our HAEs, and in this paper we use their catalogued magnitudes.

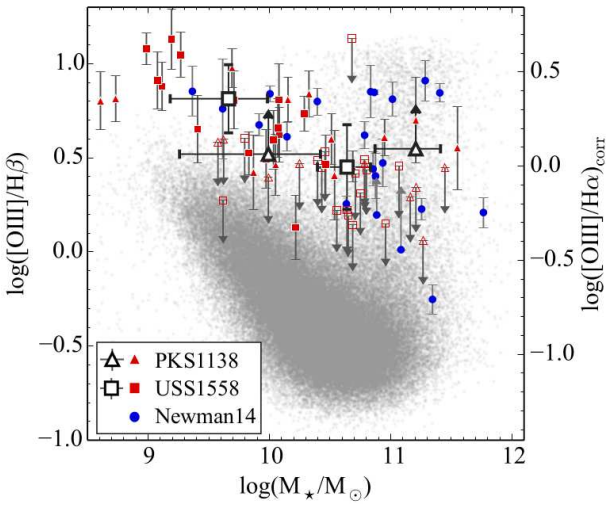

Figure 4. Mass-excitation (MEx) diagrams for individual and stacked results. White triangles and squares indicate the stacked spectra of in PKS1138 and USS1558, respectively. Red triangles, squares, and blue circles show the individual HAEs in PKS1138, USS1558, and SINS & LUCI data (field) at z=2.1–2.5 (Newman et al. 2014), respectively. [OIII]/Hβ line ratio of individual objects in PKS1138 and USS1558 is based on the prescriptions of Wuyts et al. (2013) and intrinsic Hα/Hβ flux ratio (=2.86). We show the 2σ upper limit for [OIII]-undetected ($< 2\sigma$) objects. Hβ absorption is not considered for the Newman et al. (2014) sample. Grey dots represent the SDSS galaxies with $EW_{H\alpha}$>20Å (Abazajian et al. 2009). Error-bars indicate flux errors of 1σ in the respective samples.

HAE candidates, but also detects [OIII] emission line for about a half of the confirmed HAEs. Interestingly, their [OIII] fluxes are often higher than their Hα fluxes. The fraction of [OIII] detection (50%) is much larger by about 3 times than expected from the typical [OIII]/Hα line ratio of local SF galaxies. In the local SDSS galaxies that we select in this paper, for example, ∼97% of the HAEs (i.e. EW>20Å) have [OIII] line fluxes that are smaller than Hα fluxes (without dust correction) even including Seyfert AGNs, while our HAE sample at z>2 has higher [OIII] fluxes than Hα at a rate of >43% with reddening correction. This may indicate that the SF galaxies at $z > 2$ have much higher ionization states in dense regions the same as in the field environments (e.g. Kewley et al. 2013b; Shirazi, Brinchmann & Rahmati 2014; Steidel et al. 2014).

By studying the relationship between [OIII]/Hα line ratio and stellar mass, we obtain a diagnostic which can separate Seyfert AGNs from SF galaxies. This diagram is called Mass-Excitation (MEx) diagram which was first discussed by Juneau et al. (2011). The original MEx is presented by using a close-pair line ratio, [OIII]/Hβ. However, this work alternatively employs the [OIII]/Hα line ratio for individual objects to derive [OIII]/Hβ ratio by assuming the dust extinction (UV/Hα) as presented in the previous section, because Hβ lines are rarely detected for individual galaxies.

Figure 4 shows the MEx diagram. We can see that the [OIII]/Hβ line ratios (from [OIII]/Hα) of our sample are higher by an order of magnitude than SDSS galaxies at the same stellar mass. This indicates that the ionizing states of high-z galaxies are significantly higher than low-z galaxies. Such high excitations of the protocluster galaxies at $z > 2$ are consistent with those of field galaxies as noted by recent work (Newman et al. 2014; Holden et al. 2014; Juneau et al. 2014; Coil et al. 2014). The success rate of [OIII] detection ($> 2\sigma$) is poor for high-mass galaxies and the 2σ limit flux is assigned to the objects if [OIII] line is not detected. The absence of the [OIII] line in high-mass galaxies is likely to be caused by both influence of higher dust extinction (Garn & Best 2010) and intrinsically smaller [OIII] fluxes (Nakajima & Ouchi 2014) in massive galaxies compared to lower-mass objects.

To compare our result with field galaxies at the similar redshifts, the field SF galaxies (and some X-ray sources) obtained by SINS and LUCI survey (Newman et al. 2014) are also shown. The stacked spectrum 'PKS1138-high' in the higher mass bin has a higher [OIII]/Hβ line ratio than that of 'USS1558-high' in spite of the fact that 'PKS1138-high' bin is more massive than that of 'USS1558-high'. It may be caused by a significant contribution of Seyfert-type AGNs, and indeed 'PKS1138-high' and three massive objects in PKS1138 are slightly offset to the AGN regime from the $M_\star$ vs. [OIII]/Hβ sequence which is established for field samples at $z > 2$ (Fig. 4). However, none of the HAEs in PKS1138 are detected by *Chandra* X-ray observations (Pentericci et al. 2002). At this stage, we cannot clearly identify AGN contaminations.

The [OIII]/Hβ line ratio estimated from the [OIII]/Hα assuming the intrinsic Balmer line ratio (Hβ= Hα/2.86) and correcting for dust extinction, seems to work well, since they are consistent with the direct measurement of [OIII]/Hβ line ratio derived from the stacked spectra as shown in Fig. 4. This method can be used as an alternative way to estimate the level of gaseous excitation in SF galaxies even if their Hβ lines are not available. Note however that it tends to overestimate the [OIII]/Hβ line ratios for low-mass galaxies ($<10^{10}M_\odot$), because the dust correction using UV/Hα does not work well for young galaxies due to its sensitivity to the amount of hot massive stars (Wuyts et al. 2013). Indeed we find that the [OIII]/Hβ line ratios estimated using this calibration are higher by 0.2–0.3 dex compared to their [OIII]/Hβ line ratios directly calculated by follow-up spectroscopy with the Multi-Object Spectrometer for InfraRed Exploration (MOSFIRE; McLean et al. 2012) on Keck-1 10m telescope (Shimakawa et al. in prep.). Even considering this factor, however, we can say that the protocluster galaxies also show high gaseous excitation levels, same as those of field galaxies at similar redshifts on average.

3.3 BPT diagram

The BPT diagram is the most traditional diagnostic to investigate the physical states of galaxies and identify AGN contributions (Baldwin, Phillips & Terlevich 1981). It can discriminate Seyfert AGNs from HII region-like SF galaxies based on [OIII]λ5007Å, [OI]λ6300Å, [NII]λ6583Å, [SII]λ6716 + 6731Å, and hydrogen Balmer series lines, such as H$\alpha\lambda$6563Åand H$\beta\lambda$4861Å. In principle, low-ionization nuclear emission-line regions (LINERs) are also classified as AGNs on the BPT diagram. However, our previous NB imaging originally selected HAEs with $EW_{H\alpha} > 20$Å (Koyama et al. 2013a; Hayashi et al. 2012), and the contamination of LINERs should be negligible since their $EW_{H\alpha}$ is

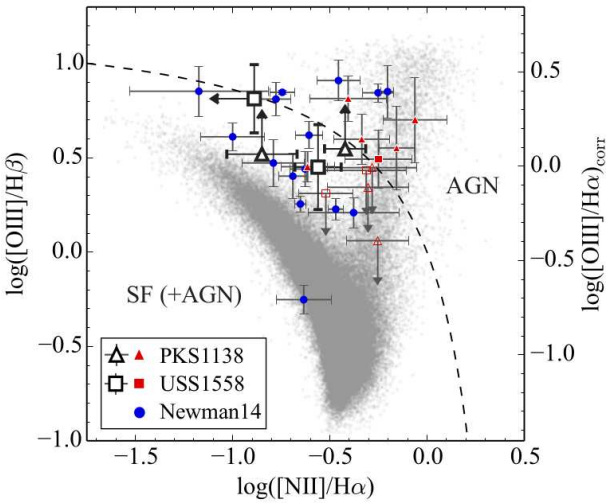

Figure 5. [NII]/ Hα versus [OIII]/ Hβ diagram (BPT diagram). White triangles and squares indicate the stacked spectra of HAEs in PKS1138 and USS1558 protoclusters, respectively. Red triangles, squares, and blue circles show the individual HAEs in PKS1138, USS1558, and SINS & LUCI data (field) at z=2.1–2.5 (Newman et al. 2014), respectively. We plot only [NII] detected objects for individual galaxies in our sample. [OIII]/ Hβ line ratios of individual objects in PKS1138 and USS1558 are estimated with the dust extinction prescription of Wuyts et al. (2013) and assuming the intrinsic Hα/ Hβ flux ratio of 2.86 (Case-B). Red open symbols show the 2σ upper limits for [OIII]-undetected ($< 2\sigma$) objects. Hβ absorption is not considered for the Newman et al. (2014) sample. Grey dots represent the SDSS galaxies with $EW_{H\alpha}$>20Å (Abazajian et al. 2009). Error-bars indicate flux errors of 1 sigma of each sample.

small (< 6Å) as they are dominated by old (red) stellar continuum (Cid Fernandes et al. 2011). In this work, we use the [NII]/ Hα versus [OIII]/ Hβ diagnostic which is more favorably used than other line diagnostics such as those using [OI] or [SII] since these lines are too weak to be detected for high redshift galaxies in most cases.

The theoretical predictions on the BPT diagram has been improved by many authors (e.g. Veilleux & Osterbrock 1987; Kewley et al. 2001; Kauffmann et al. 2003; Kewley et al. 2006). However, applicability of the BPT diagram is disputable for separating SF galaxies from AGNs. High-z galaxies, especially those at $z > 2$, are systematically offset from the tight sequence ('abundance sequence'), as [OIII]/ Hβ and/or [NII]/ Hα line ratios of $z > 2$ SF galaxies tend to be much higher than those of low-z (Erb et al. 2006a; Newman et al. 2014; Kewley et al. 2013b; Masters et al. 2014; Steidel et al. 2014). Also, the AGN branch defined at low-z on the BPT diagram seems to be shifted to the upper-left direction of the diagram at high-z (Kewley et al. 2013b,a). Kewley et al. (2013b) have newly defined the demarcation curve semi-empirically depending on redshift ($0 < z < 2.5$) on the diagram called "cosmic BPT diagram". They adjust several physical parameters such as lower gaseous metallicity, higher ionization parameter, and harder radiation field to reproduce the distant SF galaxies (and AGNs).

Figure 5 shows the BPT diagram with our data points from the stacked spectra and the individual measurements for the objects whose [NII] line is detected above 2σ. For comparison with lower-z galaxies and the field galaxies at z=2.1–2.5, we also plot other data taken from the literature (Abazajian et al. 2009; Newman et al. 2014, respectively). At $z > 2$, the chemical abundance sequence has higher [OIII]/ Hβ ratios on average than that of local SF galaxies as seen in Fig. 5. We are not able to detect a Hβ line for individual objects in the current MOIRCS spectra, and we thus estimate the [OIII]/ Hβ line ratio from the [OIII]/ Hα ratio with taking into account the dust extinction and Balmer line ratio (Hβ= Hα/2.86). For the stacked data, we measure directly Hβ/ [OIII] ratios whose extinctions are corrected by Balmer decrement.

Based on the BPT diagram, we newly find five AGN candidates in our sample. They have large [NII]/ Hα and [OIII]/ Hβ (from [OIII]/ Hα) line ratios above the criteria defined by Kewley et al. (2013b) (cosmic BPT diagram at $z = 2.5$). They have higher [NII]/ Hα and [OIII]/ Hβ line ratios as is also seen in the MEx diagram. The AGN candidates in PKS1138 are not detected in X-ray to a limit of 0.8×10^{-15} erg/s/cm^2 in the soft band (Pentericci et al. 2002), however, which may indicate that they are highly obscured AGNs. We exclude these AGN-like HAEs demarcated by this diagram from the stacked spectra hereafter, which can provide us with the information about HII region like properties of the protocluster galaxies more directly. We caution that our spectra are unable to constrain below log([NII]/ Hα)$\lesssim$-0.5.

3.4 Mass–metallicity relation

The gaseous metallicity is one of the crucial physical quantities to trace the chemical enrichment histories hence star formation histories of galaxies. There is a well established relationship between stellar-mass (or luminosity) and metallicity known as the mass–metallicity relation (M–Z relation) (Tremonti et al. 2004), and it reflects information of gas accretion, chemical nucleosynthesis and outflows of galaxies. While the metallicity increases with age, stellar-mass grows not only with age but also through galaxy-galaxy mergers. Galaxies with larger gas fractions also tend to have lower metallicities (Mannucci et al. 2010; Tadaki et al. 2013). In dense regions, we can test whether galaxies have higher metallicity (are more evolved) due to "accelerated" galaxy formation. Moreover, the gas that is ejected from a galaxy by a galactic wind may fall back on to the host galaxy on a shorter timescale in denser environments (Davé, Finlator & Oppenheimer 2011). In fact, Kulas et al. (2013) show an offset of gaseous metallicity in the low-mass protocluster galaxies ($M_\star \lesssim 10^{11} M_\odot$) at $z = 2.3$.

Gaseous metallicity can be estimated in many ways such as N2 index (Pettini & Pagel 2004), R23 (McGaugh 1991; Kobulnicky & Kewley 2004), and a direct T_e method (Izotov et al. 2006). The absolute values of metallicities depend on the method to take, and thus conversion factors are required to compare metallicities among different studies (Kewley & Ellison 2008). Several authors have compared various metallicity calibrations, and obtained consistent metallicities based on different line ratios (Nagao, Maiolino & Marconi 2006; Maiolino et al. 2008; Troncoso et al. 2014). However, the gaseous metallicity strongly correlates with the ionization parameter except for some specific line ratios such as [NII]/ [OII]

(Kewley & Dopita 2002). Also, if ISM conditions of SF galaxies change with the cosmic time as suggested by Shirazi, Brinchmann & Rahmati (2014), it makes such line diagnostics difficult and the comparison of gaseous metallicities uncertain between galaxies at different redshifts. Nakajima et al. (2013); Nakajima & Ouchi (2014) have claimed that distant galaxies at $z > 2$ have higher ionization parameter by 4 times than local galaxies, which provides a different metallicity for a given R23 value. Any reliable diagnostic for high redshift galaxies has not been established so far, and it should be noted that this work discusses only "relative" values of gaseous metallicities at similar redshift (z∼2).

We estimate a gaseous metallicity using the N2 index measured from the stacked spectrum after remaining AGN candidates (§3.3). The N2 index is defined by the following expression (Pettini & Pagel 2004),

$$12 + \log(\mathrm{O/H}) = 8.90 + 0.57\ \mathrm{N2}. \quad (4)$$

This diagnostic is quite useful and commonly used by past studies (e.g. Erb et al. 2006a) since it requires only [NII]λ6583Å and Hαλ6563Å lines. Because of the close proximity of the two lines, this index is free from uncertainties in flux calibration or dust extinction. The N2 index has been empirically calibrated with local galaxies, and it gives an unique solution of metallicity as it monotonically increases with metallicity unlike the R23 index which often gives two solutions. It is thus an useful diagnostic for a relative comparison of gaseous metallicities among galaxies.

Although Pettini & Pagel (2004) give a better fit to the data by a third-order polynomial function as also noted by Nagao, Maiolino & Marconi (2006), we here adopt eq. (4) in order to compare our results directly with previous work (Erb et al. 2006a). The [NII] line is weak for individual galaxies in our sample, but it is detected at more than 2σ significance in the stacked spectra of PKS1138 (of all mass bins) and USS1558 (only at the high mass bin).

Figure 6 shows stellar masses versus gaseous metallicities of SDSS galaxies, field galaxies at $z = 2.2$ (Erb et al. 2006a), and our protocluster galaxies measured from the stacked spectra (§2.2). The metallicities of the galaxies in the PKS1138 protocluster at $z = 2.2$ (red triangles) are systematically shifted upward by $\gtrsim$0.1 dex from the best-fit curve of the $z = 2.2$ field galaxies shown by the blue dashed curve (Erb et al. 2006a). The data point of 'USS1558-high' is also located on the same sequence of PKS1138, which suggests that the SF galaxies in both protoclusters have similar chemical abundance for a given stellar-mass. It should be noted that the stacked spectra, especially 'PKS1138-high' may be contaminated by AGNs as discussed in §3.3, which raises the [NII]/ Hα line ratio. We have therefore excluded those AGN candidates demarcated by the cosmic BPT diagram (Kewley et al. 2013b) from the stacked spectra. It has lowered the data point by ∼0.1 dex with respect to the original point of 'PKS1138-high'. As a result, we have confirmed the clear excess in gaseous metallicities in protocluster galaxies at the mass range of $\lesssim 10^{11}$ $M_\odot$. The recent result on another protocluster at z=2.3 by Kulas et al. (2013) with MOSFIRE on Keck, is consistent with our result as it also reports a higher metallicity in the dense environment than in the field.

We approximately fit the mass–metallicity relation to our sample by a second-order polynomial function as follows,

$$12 + \log(\mathrm{O/H}) = 8.46 + 0.21x - 0.07x^2, \quad (5)$$

where $x \equiv \log(M_\star/M_\odot) - 10$. We will use this calibration to estimate the contamination from [NII] line flux and subtract it from the NB flux (= Hα+ [NII]) to obtain Hα flux (§3.1).

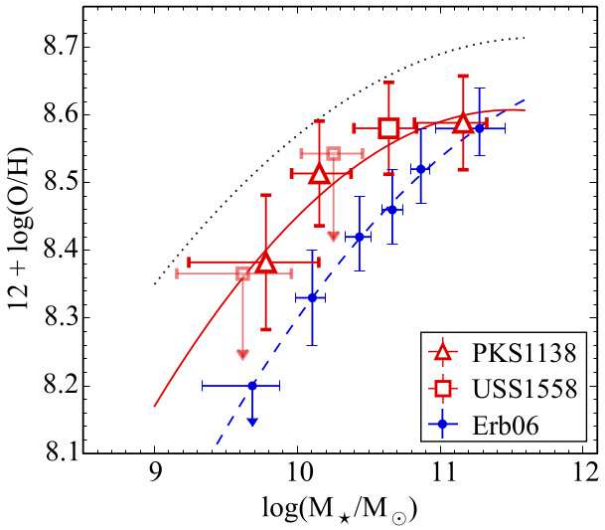

Figure 6. Stellar-mass versus gaseous metallicity diagram. We here estimate the metallicities based on the [NII]/ Hα line ratios using the empirical calibration (Pettini & Pagel 2004). Open triangles and squares indicate the stacked spectra of in PKS1138 and USS1558, respectively. Here is the revised metallicity corrected for AGN contamination based on the X-ray observation (Pentericci et al. 2002) and the cosmic BPT diagram (Kewley et al. 2013b). We employ the 2σ upper limit for [NII]-undetected ($< 2\sigma$) objects. Blue circles indicate the metallicities measured from the stacked spectra of UV-selected field galaxies at $z = 2.2$ (Erb et al. 2006a). The red and blue curves are the best-fit curves for each result. Error-bars indicate flux errors of 1 sigma in the respective samples. Dotted line represents the median of M–Z relation for SDSS galaxies at $z \sim 0.1$ with $EW_{H\alpha}$>20Å (Abazajian et al. 2009).

4 DISCUSSION

Protoclusters are the ideal laboratories to study how the strong environmental dependence in galaxy properties seen today was initially set up. Strong line ratios such as [NII]/ Hα can provide information on the formation and evolution of galaxies accelerated environments. In this section, various causal connections, implications, and speculations regarding the forming process of high-z galaxies and its environmental dependence will be discussed based on the results of this work.

4.1 High ionization states of SF galaxies at z > 2

The BPT and MEx diagrams show that the SF galaxies in the protoclusters at $z > 2$ have high ionization states even for massive objects. Such a high excitation level seen in high-z galaxies have been reported by many recent studies in the general fields (Erb et al. 2006a; Kewley et al. 2013b; Newman et al. 2014; Holden et al. 2014; Masters et al. 2014;

Steidel et al. 2014). Line-luminous galaxies actually tend to be located at the upper side of the abundance sequence on the BPT diagram (Juneau et al. 2014). It seems unlikely that this is due to an observational bias where we may be selectively sampling galaxies with higher [OIII]/ Hβ ratios with higher completeness in our $z > 2$ sample. For example Kewley et al. (2013b) have confirmed that their sample of $z > 2$ galaxies do not suffer from such a bias originated from the sensitivity limit.

What is the major intrinsic cause of the high excitation level (higher [OIII]/ Hβ ratio for a given [NII]/ Hα) at high redshifts? It can be attributed to different ISM conditions (ionization parameter, hardness of radiation field, and electron density) of high redshift SF galaxies compared to those of lower redshift counterparts as discussed in Kewley et al. (2013a); Shirazi, Brinchmann & Rahmati (2014). In this work, we discuss more quantitatively the offset of the abundance sequence at $z > 2$ based on the gaseous metallicities and the specific star-formation rates (sSFR) of Hα-selected galaxies. sSFR is also an important parameter that controls the ionization states (Shimakawa et al. 2014a), and indeed Brinchmann, Kunth & Durret (2008) have found that the SDSS galaxies with higher Hα equivalent width (almost equivalent to higher sSFR) are slightly elevated ($\sim$0.3 dex by a 3 times larger equivalent width) from the average sequence of the full-sample of SF galaxies. Furthermore, sSFR increases dramatically as we go closer to $z \sim 2$ (Daddi et al. 2007; Whitaker et al. 2012) while gaseous metallicity decreases (Erb et al. 2006a; Maiolino et al. 2008; Troncoso et al. 2014). According to Whitaker et al. (2012), sSFR of $z = 2$ SF galaxies at $\log(M_\star/M_\odot)$=10.5 is $\sim$33 times larger than that of $z = 0$ galaxies. There are few such galaxies with extremely high sSFRs in the low-z universe. It is thus considered that such significantly high sSFRs at $z \sim 2$ are probably responsible for their very high ionization states.

Figure 7a shows a BPT diagram for the SDSS galaxies. The red and blue curves show the difference in galaxy distributions on this diagram between those having higher dust-corrected sSFR ($sSFR_{corr}$) above the 1σ scatter at a given N2 index ($\equiv\log($ [NII]/ Hα) or gaseous metallicity), and those with nearly average $sSFR_{corr}$ values within $\pm1\sigma$ scatter. Here, we employ only the HII region-like galaxies in the SDSS sample within a specific redshift range (z=0.04–0.1) selected by local BPT diagram (Kewley et al. 2006) and their sSFR are based on Brinchmann et al. (2004). We can see that the [OIII]/ Hβ ratios of the galaxies with higher sSFRs (by $\sim$ 0.5 dex; see the bottom panel of Fig. 7a have systematically higher [OIII]/ Hβ ratio by $\sim$ 0.1 dex for a given N2 i.e. metallicity on average).

On the other hand, Fig. 7b represents the dust-corrected sSFR ($sSFR_{corr}$) versus [OIII]/ Hβ line ratio and their difference in galaxy distribution on the diagram between those having lower N2$\equiv\log($ [NII]/ Hα) (lower than 1σ scatter at a given $sSFR_{corr}$) and those having nearly averaged N2 values within $\pm1\sigma$. Our HAEs in the protocluster are over-plotted in this diagram by filled triangles and squares. $sSFR_{corr}$ are derived from the NB fluxes with the dust correction based on UV/ Hα ratios (§3.1). The [OIII]/ Hβ line ratios are estimated from the [OIII]/ Hα line ratios using the dust correction prescription based on UV/ Hα ratios (§3.2). This method works well since it is consistent with the direct

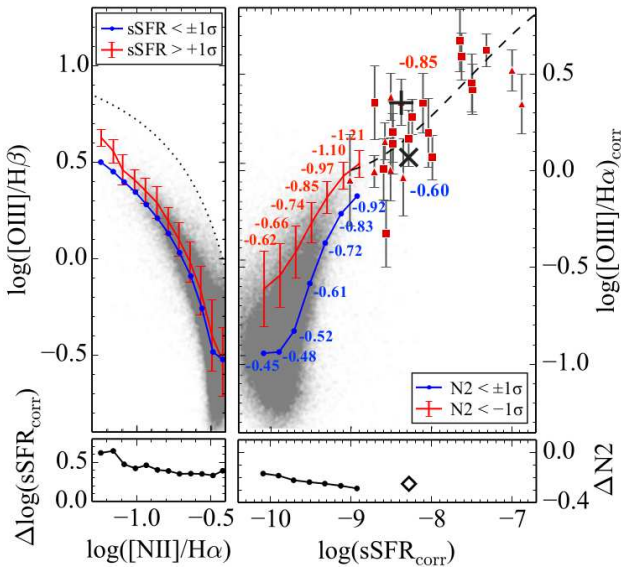

Figure 7. (a) Left: [NII]/ Hα versus [OIII]/ Hβ diagram (BPT diagram). Grey dots show the SDSS galaxies at $0.04\leqslant z\leqslant0.1$ (Abazajian et al. 2009). The blue curve shows the average values of the [OIII]/ Hβ ratios as a function of N2 index (= [NII]/ Hα ratio or metallicity) for the SDSS galaxies whose sSFRs are within $\pm1\sigma$ scatter (nearly averaged values) for a given [NII]/ Hα ratio, while the red curve shows the average values of those whose sSFRs are higher than $+1\sigma$ values. The error-bars on the red curve show $\pm1\sigma$ scatter of the [OIII]/ Hβ ratios. The difference in log(sSFR) of the two samples is displayed in the lower panel. (b) Right: log(sSFR) versus [OIII]/ Hβ diagram. Grey dots show the SDSS galaxies (same as those in the left panel). The blue curve shows the average values of [OIII]/ Hβ ratios as a function of sSFR for the SDSS galaxies whose N2 indices (hence metallicity) are within $\pm1\sigma$ scatter (nearly averaged values) for a given sSFR, while the red curve shows the average values of those whose N2 indices are smaller than -1σ values. The error-bars on the red curve show $\pm1\sigma$ scatter of the [OIII]/ Hβ ratios. The difference in N2 values of the two samples is displayed in the lower panel. Filled triangles and squares indicate our measurements for the individual HAEs in PKS1138 and USS1558 protoclusters, respectively. We note that the individual [OIII]/ Hβ line ratios are actually derived from the [OIII]/ Hα ratios, by estimating the dust extinction based on the UV/ Hα ratios (which we know are consistent with the Balmer decrement measurements from the stacked spectra (see §3.2). The "+" and "×" symbols represent the median values for the two samples of HAEs separated by the dashed line which is the best-fit line to our sample. The averaged N2 values are indicated by small numbers at each bin, including the above two HAE samples (measured from the stacked spectra for our data). Note that for a given sSFR, those having higher [OIII]/ Hβ ratios have lower N2 values, indicating that gaseous metallicities are also contributing to high [OIII]/ Hβ ratios of the HAEs in the protoclusters as well as high sSFRs.

mesurements of [OIII]/ Hβ ratio for the stacked spectra (§3.2). Interestingly, the HAEs in the protoclusters at $z > 2$ more or less follow the extension of the correlation between sSFR vs. [OIII]/ Hβ for the SDSS galaxies. Such trend is also reported in a recent paper (Holden et al. 2014), but our sample covers a wider stellar-mass range ($9\lesssim\log(M_\star/M_\odot)\lesssim12$). In fact, our protocluster galaxies at $z > 2$ have much higher sSFRs (by 1–2 orders of magnitude) as well as much higher [OIII]/ Hβ ratios compared to the SDSS galaxies. This sug-

gests that sSFR is a key factor that raises the [OIII]/ Hβ line ratios. Moreover, the ratios also depend on the gaseous metallicity in the sense that lower [NII]/ Hα ratios (N2 values) hence lower metallicities raise the [OIII]/ Hβ line ratios for a given fixed sSFR. Therefore, the significant offset of the high-z SF galaxies on the BPT diagram is likely to be caused by their both higher sSFRs and lower metallicities compared to those of local galaxies. Lower metallicities shift the galaxies to the upper left direction on the BPT diagram (lower [NII]/ Hα and higher [OIII]/ Hβ) (Kewley et al. 2013a). Also, higher sSFRs raise the [OIII]/ Hβ line ratios further at a given metallicity (N2).

Although Fig. 7 apparently shows a smooth correlation between log sSFR and [OIII]/ Hβ ratio, there is a large gap of 0.5 dex between the local SDSS galaxies and our samples of high-z SF galaxies when we compare them at a fixed [NII]/ Hα line ratio. It suggests that some other factors may be contributing to the offset of the high-z galaxies on the BPT diagram such as the effects of outflows (Whitaker et al. 2014), N/O enhancement by Wolf-Rayet stars (Masters et al. 2014), and/or higher gas pressure in high-z galaxies (Shirazi, Brinchmann & Rahmati 2014). We cannot resolve this problem from this result alone, and further details are beyond the scope of this paper.

4.2 Environmental dependence of galaxy formation at z > 2

The PKS1138 and USS1558 are the largest class of protocluster at $z = 2.2$ and $z = 2.5$, respectively which are likely to grow to a massive cluster of a total mass of $\sim 10^{15}$ $M_\odot$ by the present-day (Shimakawa et al. 2014b). As such it is the ideal place to test the environmentally dependent galaxy formation in the early epoch. We have compared the physical states and the gaseous metallicities of HAEs in the protoclusters at z=2.2 and 2.5 with those in the general fields to address the environmental dependence in galaxy formation. Our data cover a wide range in stellar mass, i.e. $\log(M_\star/M_\odot)$=9–12, which enables us to investigate the mass dependence of the environmental dependency as well.

Generally, the outflow of chemically-enriched gas can reduce gaseous metallicity in galaxies, while the inflow of primordial gas also dilutes the metallicity (Erb et al. 2006a; Erb 2008; Dalcanton 2007; Mannucci et al. 2009). The upward shift by 0.1–0.15 dex of the M–Z relation in the protoclusters with respect to that of the general field at $z \sim 2$ indicates that the chemical evolution proceeds faster in the dense environment at a given stellar mass. Recently, Kulas et al. (2013) first noted the excess of gaseous metallicities of SF galaxies in the protocluster HS1700+643 ($z = 2.3$) as compared to the general field, at the stellar mass range of $\log(M_\star/M_\odot) \lesssim 11$. This is consistent with our result (§3.4). The reasons for such an offset of the M–Z relation in the protocluster at $z > 2$ have five possibilities, namely, (1) recycling of chemically enriched gas due to higher pressure of inter galactic medium (external or nurture effect) (Davé, Finlator & Oppenheimer 2011; Kulas et al. 2013), (2) stripping of metal poor HI gas loosely trapped in the outer reservoirs by galaxy-galaxy interactions or ram-pressure (external or nurture effect) (3) advanced stage of down-sizing galaxy evolution (intrinsic or nature effect) (Thomas et al. 2005), (4) top-heavy IMF in young star-bursting phase, and (5) sample selection bias.

(1) First of all, the environmentally dependent recycling of chemically enriched gas is discussed by Kulas et al. (2013). They suggest that the metal enhancement seen in the over-dense regions can be accounted for by a fall-back and a recycling of ejected outflowing gas due to higher pressures of the surrounding inter galactic medium (IGM) in clusters. Recycling of chemically enriched gas leads to the formation of next generation of stars and thus chemical evolution would be proceeded further in clusters. Such phenomenon is predicted by numerical hydrodynamical simulations by Oppenheimer & Davé (2008); Davé, Finlator & Oppenheimer (2011). In this scenario, the metal enhancement depends not only on the IGM density hence the richness of clusters, but also on the dynamical mass of individual galaxies. Such differential chemical evolution between different environments must be more prominent for less massive galaxies because massive galaxies have larger potential wells and the gas tends to be retained and easier to be recycled in any case irrespective of their surrounding environments. This is favored by the observations which indicate a lack of environmental dependence of metallicities in massive galaxies.

(2) Secondly, once an in-falling galaxy is incorporated into a common cluster halo, the gas reservoir of the galaxy may be stripped or truncated due to the interactions with cluster potential, intra-cluster gas, and/or other galaxies (Abadi, Moore & Bower 1999; McCarthy et al. 2008). This can not only expel low metallicity gas trapped in the outer region of the galaxy, but also terminate the fresh gas accretion onto the galaxy which would have otherwise diluted the high metallicity gas at the center in the infall dominated phase of galaxy formation ($z > 2$). Therefore, we expect that this process can effectively increase the gaseous metallicity of galaxies in cluster environment, as compared to isolated galaxies.

(3) Thirdly, there is an intrinsic (nature) effect that the timescale of galaxy evolution depends on environment, because densest environments such as clusters of galaxies start off from the highest density peaks in the early Universe which must collapse first. Because of this bias, galaxy formation and evolution should proceed earlier and/or faster, so does the chemical evolution. In this case, the environmental dependence of gaseous metallicity seen particularly in lower mass galaxies can be naturally explained by environmentally dependent galaxy downsizing (mass dependent timescale of galaxy formation and evolution, Cowie et al. 1996; Cattaneo et al. 2008), in the sense that the downsizing proceeds earlier in the protocluster regions, and hence the gas in protocluster galaxies are more chemically enriched for a given stellar mass especially in less massive galaxies.

One should note, however, that we are comparing metallicities between different environments at a given 'stellar' mass, and not at a fixed total or 'halo' mass including 'gas' mass. The same amount of stellar mass means that they have synthesized the same absolute amount of metals. However, the gaseous metallicity (O/H) depends on gas content or fraction as well. Cluster galaxies can have the same stellar mass as the field galaxies but with smaller gas fraction and thus smaller total baryonic or halo masses, because of the

more advanced downsizing effect. Basically, we may be comparing between the advanced stage of galaxies with low halo masses in clusters with the less advanced stage of galaxies with high halo masses in the field. Such difference is expected to be seen more prominently in less massive systems, since massive galaxies are already well evolved irrespective of their environments, and we do not expect to see a sizable difference in the evolutionary stage hence gaseous metallicity for massive galaxies.

This scenario, however, has a contradiction. Because the advanced evolutionary stage should mean smaller gas fraction for cluster galaxies for a given stellar mass, we would expect them to have lower specific sSFRs compared to those of field galaxies. This is not consistent with the observational results of Koyama et al. (2013a,b) who show the environmental independence of sSFRs.

(4) A top heavy IMF for cluster galaxies can also explain the metallicity excess since it increases the intrinsic chemical yield. The top-heavy IMF is actually preferred to account for high (α/Fe) ratios of massive early-type galaxies (e.g. Baugh et al. 2005; Nagashima et al. 2005a,b). However, the metallicity difference is seen only in low mass galaxies, and so this scenario is not favored.

(5) Finally, different sample selections may be an issue between this work (protoclusters) and Erb et al. (2006a) (general field). Our NB selection of SF galaxies based on Hα emission line can cover a broader range of SF galaxies in terms of stellar-mass. Also the dust obscuration effect can be minimized. On the contrary, the UV-selected SF galaxies by Erb et al. (2006a) tend to be biased to less dusty and relatively young populations (see also Steidel et al. 2004). This may result in an apparent difference in the M–Z relation between the two samples as discussed by Stott et al. (2013) at z=0.8–1.5. These two samples correspond to different stages of galaxy evolution in the sense that Hα selected galaxies are in a more advanced stage hence could be chemically more enriched at a given stellar mass. However, there is no environmental dependence between field and cluster galaxies at $z \sim 2$ as reported by Koyama et al. (2013a,b). Moreover, the offset we see in the M–Z relation for the protocluster galaxies (0.1–0.15 dex) cannot be accounted for by the sampling bias alone that Stott et al. (2013) claim. In fact, for the SDSS galaxies, the amount of dust extinction is largely determined by the stellar mass, and at the fixed stellar mass we do not see any clear dependence of the deviation from the M–Z relation on the amount of dust extinction (see Appendix, and also Zahid et al. 2014b). Therefore, we do not expect a strong selection bias between the UV selected SF galaxies (Erb et al. 2006a) and the Hα selected samples (this work). Furthermore, the fact that we do not see the metallicity offset for massive galaxies which tend to be more heavily obscured also suggest that the sampling bias should not be the main reason for the offset of the M–Z relation for low mass galaxies.

Following the above discussions, we suggest that the offset in gaseous metallicity in dense regions may be driven by the environmental dependence of "feeding & feedback" processes of galaxy formation at high redshifts. Cluster galaxies are formed within complicated structures such as clusters, surrounding groups, filaments and sheets, as simulated by CDM-dominated cosmological simulations (e.g. Springel et al. 2005). Also, recent models predict that the cold gas accretion is the dominant gas supply mechanism in high redshift galaxies, and that such process of gas inflow depends strongly on halo mass and redshift (Dekel et al. 2009). Moreover, other models simulate gas outflow processes which are dependent on galaxy mass and surrounding environment (Davé, Finlator & Oppenheimer 2011). Therefore, it is natural that cluster galaxies follow different tracks of chemical evolution from the field ones in their vigorous formation phase.

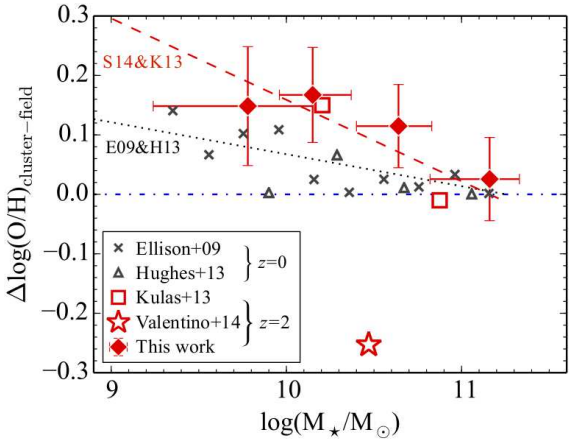

Figure 8. The offset of the averaged gaseous metallicities 12+log(O/H) of protocluster/cluster galaxies from those in general fields in the literature plotted against stellar mass. Red diamonds, squares, and a star indicate SF galaxies at $z \sim 2$ in dense regions reported by this work and Kulas et al. (2013); Valentino et al. (2014), respectively. Grey crosses and triangles show local SF galaxies in dense regions above $\Sigma > 1$ Mpc^{-2} based on SDSS sample (Ellison et al. 2009) and in Virgo cluster (Hughes et al. 2013), respectively. Dotted and dashed lines are the fitted lines where Δlog(O/H) is set to be zero at log(M$_\star$/M$_\odot$)=11.16 for both local and the $z \sim 2$ samples except for the Valentino et al. (2014) data.

Figure 8 represents the offset of gaseous metallicities of the cluster galaxies from those of field counterparts. Here, we collect $z \sim 2$ samples from Kulas et al. (2013); Valentino et al. (2014) include this work, and local samples from Ellison et al. (2009) (SDSS galaxies in dense region above $\Sigma > 1$ Mpc^{-2}) and Hughes et al. (2013) (Virgo cluster). We clearly see a metallicity enhancement by 0.15 dex around M$_\star > 10^{10}$ M$_\odot$ in this work, which is consistent with the earlier result by Kulas et al. (2013). Ellison et al. (2009) also reports such an excess of gaseous metallicity in cluster regions at $z \sim 0.1$ (see also Peng & Maiolino 2014). Interestingly, the offset of the M–Z relation in dense regions gets larger at $z \sim$2 (Fig. 8). This can be explained by the fact that gas transfer processes such as inflow and outflow are more active at $z \sim 2$ than those at low redshift (Steidel et al. 2010; Bouché et al. 2013; Yabe et al. 2014a). It should be noted however that this gives only a partial explanation for the environmental dependence. In fact, Valentino et al. (2014) recently reports a completely opposite trend for another overdensity region at $z = 2$.

Moreover, we need to consider SF activities of these protocluster galaxies at the same time. The gas stripping in protoclusters, if present, would lower the gas fraction,

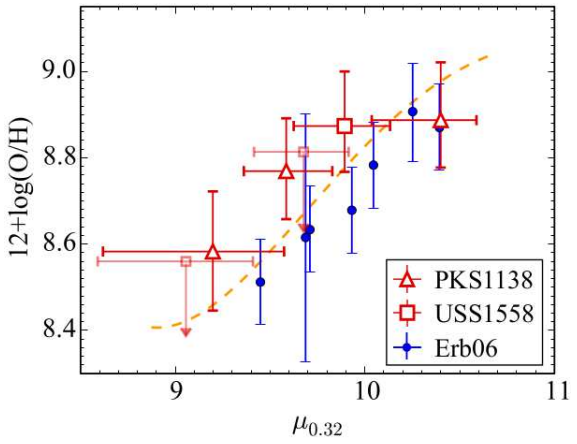

Figure 9. The fundamental metallicity relation (FMR), $\mu_{0.32}$ versus 12+log(O/H), where $\mu_{0.32}\equiv\log(M_\star)-0.32\ \log(SFR)$. Red triangles and squares indicate the protoclusters, PKS1138 at $z = 2.2$ and USS1558 at $z = 2.5$, respectively. Here we employ the Maiolino et al. (2008) calibrations for a direct comparison with the FMR of Mannucci et al. (2010). Blue circles show the field galaxies at $z = 2.2$ (Erb et al. 2006a), although their gaseous metallicities have been revised by Maiolino et al. (2008). The orange curve shows the FMR reported by Mannucci et al. (2010).

and thus lead to lower SFRs compared to field galaxies (Balogh, Navarro & Morris 2000; Kodama & Bower 2001). However, our samples of HAEs show similar SFRs irrespective of environment, and the protocluster galaxies share the same main-sequence of field SF galaxies. In the current studies we have to rely on the stacking analyses, which have lost information of any scatter among individual galaxies. Since the environmental effects are rather stochastic, a considerable scatter in the chemical properties would be expected. Therefore investigating the environmental dependence of chemical evolution on individual galaxy basis is essential as the next step.

4.3 Fundamental metallicity relation

We finally discuss the fundamental metallicity relation (FMR) of the protocluster galaxies. Mannucci et al. (2010) show that the scatter around the M–Z relation is mainly driven by the correlation between SFR and metallicity at a given stellar mass (see also Mannucci, Salvaterra & Campisi 2011; Bothwell et al. 2013; Stott et al. 2013; Yabe et al. 2014b; Troncoso et al. 2014) in the sense that galaxies with higher SFRs tend to have lower metallicities. The FMR is thus expressed as $12+\log(O/H)=\log(M_\star/M_\odot)-0.32\ \log(SFR)$ ($\equiv\ \mu_{0.32}$) and it has a scatter of only 0.05 dex. Moreover, the form of FMR seems unchanged out to $z \sim 2.5$ (Mannucci et al. 2010), and probably to $z \gtrsim 3$ as traced by Lyman break galaxies (Nakajima et al. 2013; Nakajima & Ouchi 2014, but see also Mannucci et al. 2010; Troncoso et al. 2014; Steidel et al. 2014; Sanders et al. 2014). This means that most of the SF galaxies can evolve only on the FMR and that star formation and chemical enrichment in galaxies are well regulated through secular processes across the large redshift range.

An obvious extension of such studies is to investigate the environmental dependence of the FMR at high redshift to test whether the chemical enrichment history, and thus the regulation laws among star formation, inflow, and outflow, are accelerated in dense environments. According to Magrini et al. (2012), any difference in the FMR cannot be seen for cluster galaxies at $z = 1.4$. We now show the results for higher redshift clusters at $z > 2$ where massive galaxies are growing rapidly (Kodama et al. 2007). During this epoch of galaxy formation, galaxies may go through violent, unstable phases such as massive gas infall (Dekel et al. 2009), outflows by SF/AGN feedback, and galaxy-galaxy mergers (Gottlöber, Klypin & Kravtsov 2001), which are all possibly environmentally dependent. Such environmental effects may have some impacts on chemical evolution that are different from those driven by secular processes, and thus produce an environmental variation of the FMR.

Figure 8 represents $\mu_{0.32}$ versus gaseous metallicities of HAEs in the protoclusters and those in the general field (Erb et al. 2006a; Mannucci et al. 2010). We have revised the gaseous metallicities based on the Maiolino et al. (2008) prescription ([NII]/ Hα ratio) instead of the Pettini & Pagel (2004) method, in order to directly compare the metallicities of our sample with those by (Mannucci et al. 2010) with the same method.

$$\mathrm{N2} = -0.773 + 1.236x - 0.281x^2 - 0.720x^3 - 0.333x^4 \quad (6)$$

Here, x is 12+log(O/H). We adopt the median values of stellar mass and SFR at each bin, and the error-bars indicate 1σ scatters of the stacked spectra. Our protocluster data are located above the fundamental plane (orange curve) by 0.10–0.15 dex at $\mu_{0.32} \lesssim 10$ although the plots except 'PKS1138-mid' are still consistent within the errors. The slight (∼0.10–0.15) offset of the FMR of the protocluster galaxies is caused by the metal enhancement at the stellar mass smaller than $10^{11}M_\odot$. It should be noted that the extinction correction is different between this work and Erb et al. (2006a), and our plots would be shifted rightward by $\lesssim 0.1$ dex if we adopt the same dust correction prescription by Erb et al. (2006a) (see also Erb et al. 2006b). Because of too large errorbars, however, we cannot constrain the FMR of the protocluster galaxies.

Moreover, there are some additional caveats for the investigation of the fundamental metallicity relation. Firstly, the high-z SF galaxies have higher ionization parameters and higher electron densities, which may lead us to have a systematic error in gaseous metallicity measurement (Nakajima & Ouchi 2014). For example, Steidel et al. (2014) show that the abundance measurement of a high-z galaxy based on N2 index tend to be an overestimation compared to the direct measurement based on the T_e method (Izotov et al. 2006). Secondly, we see no clear dependence of the M–Z relation on SFR in the recent works (Steidel et al. 2014; Sanders et al. 2014). Therefore it may be too early to discuss the environmental dependence of the fundamental metallicity relation yet.

5 CONCLUSIONS

This paper reports the results on the physical properties of HAEs in two protoclusters, PKS1138 at $z = 2.2$ and USS1558 at $z = 2.5$, based on the NIR spectroscopy with

Table 3. Final catalogue of the stacked spectra of HAEs in PKS1138 and USS1558 separated into two stellar mass bins (low and high) and the same stellar-mass bin for comparing with each protocluster (mid). We here exclude AGN candidates (see §3.3) from the sample. (1) ID categorized by stacking method, (2) the median stellar-mass, (3)–(4) line ratios of median stacked spectra, (5) gaseous metallicities derived from PP04 (N2 index), and (6) dust extinction of Hα calculated by using Balmer decrement. All errors are derived from 1σ scatters of respective emission line fluxes.

ID (1)	$\log(M_\star/M_\odot)$ (2)	$\log([\mathrm{NII}]/\mathrm{H}\alpha)$ (3)	$\log([\mathrm{OIII}]/\mathrm{H}\beta)$ (4)	12+log(O/H) (5)	$A_{\mathrm{H}\alpha}$ (6)
PKS1138-low	$9.78^{+0.37}_{-0.54}$	-0.91 ± 0.17	> 0.42	8.38 ± 0.10	> 2.06
PKS1138-high	$11.16^{+0.17}_{-0.34}$	-0.55 ± 0.12	> 0.19	8.59 ± 0.07	> 1.96
USS1558-low	$9.62^{+0.34}_{-0.46}$	< -0.94	0.87 ± 0.18	< 8.37	1.28 ± 1.15
USS1558-high	$10.64^{+0.19}_{-0.24}$	-0.56 ± 0.12	0.45 ± 0.22	8.58 ± 0.07	1.72 ± 1.41
PKS1138-mid	$10.15^{+0.22}_{-0.19}$	-0.68 ± 0.14	> 0.34	8.51 ± 0.08	> 0.78
USS1558-mid	$10.25^{+0.20}_{-0.23}$	< -0.63	> 0.51	< 8.54	> 1.10

MOIRCS on Subaru. We investigate the environmental dependence of the physical properties of SF galaxies to test whether how the SF activity is intrinsically biased in the dense environments, and how they are affected by their surroundings at the peak epoch of galaxy formation.

– We measure the strength of dust attenuation of HAEs using Balmer decrement ($\mathrm{H}\alpha/\mathrm{H}\beta$) from the stacked spectra and SFR($\mathrm{H}\alpha$)/SFR(UV) ratios of individual galaxies. We then investigate their physical properties with an aid of the MEx diagram (Juneau et al. 2011, 2014) and find that the ionization states of the protocluster galaxies at $z > 2$ is much higher than those of the field galaxies by an order magnitude based on their $[\mathrm{OIII}]/\mathrm{H}\beta$ or $[\mathrm{OIII}]/\mathrm{H}\alpha$ line ratios. This is consistent with many other recent works on SF galaxies at $z > 2$ in general fields (Erb et al. 2006a; Kewley et al. 2013b,a; Troncoso et al. 2014; Newman et al. 2014; Masters et al. 2014; Steidel et al. 2014; Shapley et al. 2014; Coil et al. 2014). Such a high gaseous excitation may be primarily driven by their low metallicities and very high sSFRs as shown in Figure 7. However, this is not a comprehensive explanation for the high ionization of the $z \sim 2$ galaxies, and some other effects would be needed as well (Shirazi, Brinchmann & Rahmati 2014; Masters et al. 2014; Wuyts et al. 2014).

– The history of chemical enrichment provides us with information on the physical processes that are occurring during the epoch of galaxy formation. We explore the environmental dependency of the gaseous metallicity using the N2 index (Pettini & Pagel 2004). We exclude the AGN contamination by using the BPT diagram ($[\mathrm{NII}]/\mathrm{H}\alpha$ vs. $[\mathrm{OIII}]/\mathrm{H}\alpha$) and X-ray data. We find that the protocluster galaxies of low masses ($\lesssim 10^{11}$ $M_\odot$) tend to be more chemically enriched than the field counterparts at $z = 2.2$ (Erb et al. 2006a). In order to account for the environmental dependence in the M–Z relation, we discuss five possible scenarios, including recycling of chemically enriched gas and/or stripping of metal poor gas in the reservoir. Among them, we suggest that the metal enhancement is most likely caused by the environmental effects on feeding & feedback processes during galaxy formation. The higher offset of the M–Z relation observed in dense environments at $z \sim 2$ with respect to the local relation can be explained by very active inflow and outflow processes at that epoch (Steidel et al. 2010; Bouché et al. 2013; Yabe et al. 2014a). This scenario is also supported by some theoretical works (e.g. Davé, Finlator & Oppenheimer 2011). However, we have not yet reached to any fully consistent picture from the chemical evolution alone which can also account for the SF activities in protocluster galaxies. Further investigations, both observationally and theoretically, are clearly needed.

The largest limitation of our current study is that we cannot derive gaseous metallicities for individual HAEs, and we have to rely on the stacking spectral analysis which gives us only averaged metallicities in each stellar mass bins. This cannot resolve the "heterogeneity" of chemical evolution in SF galaxies in dense environments in their early formation phase. We need deeper spectroscopy which allows us to detect multiple emission lines in each galaxy and measure its metallicity with the ISM condition also taken into account. More specifically, ionization parameter can be estimated by $[\mathrm{OIII}]/[\mathrm{OII}]$ or $[\mathrm{NeIII}]/[\mathrm{OII}]$ ratios (Levesque & Richardson 2014), and electron densities can be derived directly from $[\mathrm{OII}]\lambda3729/3726$ or $[\mathrm{SII}]\lambda6716/6731$ ratios (Puech et al. 2006; Krabbe et al. 2014; Shimakawa et al. 2014a). Such observations have just become possible by the advanced NIR multi-object spectrographs such as MOSFIRE on Keck.

ACKNOWLEDGMENTS

This paper is based on the data collected at Subaru Telescope, which is operated by the National Astronomical Observatory of Japan. We acknowledge Dr. K. Aoki and Dr. K. Yabe at Subaru Telescope for useful discussion. This work is financially supported in part by a Grant-in-Aid for the Scientific Research (Nos. 21340045 and 24244015) by the Japanese Ministry of Education, Culture, Sports, Science and Technology. We thank the referee for acknowledgements and kind help to improve the statement.

REFERENCES

Abadi M. G., Moore B., Bower R. G., 1999, MNRAS, 308, 947

Abazajian K. N. et al., 2009, ApJS, 182, 543

Adelberger K. L., Steidel C. C., Shapley A. E., Hunt M. P., Erb D. K., Reddy N. A., Pettini M., 2004, ApJ, 607, 226
Baldwin J. A., Phillips M. M., Terlevich R., 1981, PASP, 93, 5
Balogh M. L., Navarro J. F., Morris S. L., 2000, ApJ, 540, 113
Baugh C. M., Lacey C. G., Frenk C. S., Granato G. L., Silva L., Bressan A., Benson A. J., Cole S., 2005, MNRAS, 356, 1191
Bothwell M. S., Maiolino R., Kennicutt R., Cresci G., Mannucci F., Marconi A., Cicone C., 2013, MNRAS, 433, 1425
Bouché N., Murphy M. T., Kacprzak G. G., Péroux C., Contini T., Martin C. L., Dessauges-Zavadsky M., 2013, Science, 341, 50
Bournaud F., Jog C. J., Combes F., 2007, A&A, 476, 1179
Bower R. G., Kodama T., Terlevich A., 1998, MNRAS, 299, 1193
Brinchmann J., Charlot S., White S. D. M., Tremonti C., Kauffmann G., Heckman T., Brinkmann J., 2004, MNRAS, 351, 1151
Brinchmann J., Kunth D., Durret F., 2008, A&A, 485, 657
Brinchmann J., Pettini M., Charlot S., 2008, MNRAS, 385, 769
Brocklehurst M., 1971, MNRAS, 153, 471
Butcher H., Oemler, Jr. A., 1984, ApJ, 285, 426
Calzetti D., Armus L., Bohlin R. C., Kinney A. L., Koornneef J., Storchi-Bergmann T., 2000, ApJ, 533, 682
Cappellari M. et al., 2011, MNRAS, 416, 1680
Cattaneo A., Dekel A., Faber S. M., Guiderdoni B., 2008, MNRAS, 389, 567
Chabrier G., 2003, PASP, 115, 763
Cid Fernandes R., Stasińska G., Mateus A., Vale Asari N., 2011, MNRAS, 413, 1687
Coil A. L. et al., 2014, ArXiv e-prints
Cowie L. L., Songaila A., Hu E. M., Cohen J. G., 1996, AJ, 112, 839
Daddi E. et al., 2007, ApJ, 670, 156
Dalcanton J. J., 2007, ApJ, 658, 941
Davé R., Finlator K., Oppenheimer B. D., 2011, MNRAS, 416, 1354
Dekel A. et al., 2009, Nature, 457, 451
Dopita M. A., Kewley L. J., Heisler C. A., Sutherland R. S., 2000, ApJ, 542, 224
Dressler A. et al., 1997, ApJ, 490, 577
Dressler A., Oemler, Jr. A., Sparks W. B., Lucas R. A., 1994, ApJ, 435, L23
Dyson J. E., Williams D. A., 1980, Physics of the interstellar medium. (Manchester University Press)
Ebizuka N. et al., 2011, PASJ, 63, 605
Ellison S. L., Simard L., Cowan N. B., Baldry I. K., Patton D. R., McConnachie A. W., 2009, MNRAS, 396, 1257
Erb D. K., 2008, ApJ, 674, 151
Erb D. K., Pettini M., Shapley A. E., Steidel C. C., Law D. R., Reddy N. A., 2010, ApJ, 719, 1168
Erb D. K., Shapley A. E., Pettini M., Steidel C. C., Reddy N. A., Adelberger K. L., 2006a, ApJ, 644, 813
Erb D. K., Steidel C. C., Shapley A. E., Pettini M., Reddy N. A., Adelberger K. L., 2006b, ApJ, 647, 128
Ezer D., Cameron A. G. W., 1971, Ap&SS, 14, 399
Garn T., Best P. N., 2010, MNRAS, 409, 421
Gottlöber S., Klypin A., Kravtsov A. V., 2001, ApJ, 546, 223
Hayashi M., Kodama T., Koyama Y., Tadaki K.-I., Tanaka I., 2011, MNRAS, 415, 2670
Hayashi M., Kodama T., Tadaki K.-i., Koyama Y., Tanaka I., 2012, ApJ, 757, 15
Holden B. P. et al., 2014, ArXiv e-prints
Hopkins P. F., Hernquist L., Cox T. J., Kereš D., 2008, ApJS, 175, 356
Hughes T. M., Cortese L., Boselli A., Gavazzi G., Davies J. I., 2013, A&A, 550, A115
Ichikawa T. et al., 2006, in Society of Photo-Optical Instrumentation Engineers (SPIE) Conference Series, Vol. 6269, Society of Photo-Optical Instrumentation Engineers (SPIE) Conference Series
Izotov Y. I., Stasińska G., Meynet G., Guseva N. G., Thuan T. X., 2006, A&A, 448, 955
Juneau S. et al., 2014, ApJ, 788, 88
Juneau S., Dickinson M., Alexander D. M., Salim S., 2011, ApJ, 736, 104
Kashino D. et al., 2013, ApJ, 777, L8
Kauffmann G. et al., 2003, MNRAS, 346, 1055
Kennicutt, Jr. R. C., 1998, ARA&A, 36, 189
Kewley L. J., Dopita M. A., 2002, ApJS, 142, 35
Kewley L. J., Dopita M. A., Leitherer C., Davé R., Yuan T., Allen M., Groves B., Sutherland R., 2013a, ApJ, 774, 100
Kewley L. J., Dopita M. A., Sutherland R. S., Heisler C. A., Trevena J., 2001, ApJ, 556, 121
Kewley L. J., Ellison S. L., 2008, ApJ, 681, 1183
Kewley L. J., Groves B., Kauffmann G., Heckman T., 2006, MNRAS, 372, 961
Kewley L. J., Maier C., Yabe K., Ohta K., Akiyama M., Dopita M. A., Yuan T., 2013b, ApJ, 774, L10
Kobulnicky H. A., Kewley L. J., 2004, ApJ, 617, 240
Kodama T., Balogh M. L., Smail I., Bower R. G., Nakata F., 2004, MNRAS, 354, 1103
Kodama T., Bower R. G., 2001, MNRAS, 321, 18
Kodama T., Hayashi M., Koyama Y., Tadaki K.-i., Tanaka I., Shimakawa R., 2013, in IAU Symposium, Vol. 295, IAU Symposium, Thomas D., Pasquali A., Ferreras I., eds., pp. 74–77
Kodama T., Tanaka I., Kajisawa M., Kurk J., Venemans B., De Breuck C., Vernet J., Lidman C., 2007, MNRAS, 377, 1717
Koyama Y., Kodama T., Shimasaku K., Hayashi M., Okamura S., Tanaka I., Tokoku C., 2010, MNRAS, 403, 1611
Koyama Y., Kodama T., Tadaki K.-i., Hayashi M., Tanaka I., Shimakawa R., 2014, ArXiv e-prints
Koyama Y., Kodama T., Tadaki K.-i., Hayashi M., Tanaka M., Smail I., Tanaka I., Kurk J., 2013a, MNRAS, 428, 1551
Koyama Y. et al., 2013b, MNRAS, 434, 423
Krabbe A. C., Rosa D. A., Dors O. L., Pastoriza M. G., Winge C., Hägele G. F., Cardaci M. V., Rodrigues I., 2014, MNRAS, 437, 1155
Kriss G., 1994, Astronomical Data Analysis Software and Systems, 3, 437
Kulas K. R. et al., 2013, ApJ, 774, 130
Kurk J. D., Pentericci L., Röttgering H. J. A., Miley G. K., 2004, A&A, 428, 793
Kurk J. D. et al., 2000, A&A, 358, L1
Larson R. B., 1981, MNRAS, 194, 809
Levesque E. M., Richardson M. L. A., 2014, ApJ, 780, 100

Maeder A., 1987, A&A, 178, 159
Magrini L., Sommariva V., Cresci G., Sani E., Galametz A., Mannucci F., Petropoulou V., Fumana M., 2012, MNRAS, 426, 1195
Maiolino R. et al., 2008, A&A, 488, 463
Mannucci F., Cresci G., Maiolino R., Marconi A., Gnerucci A., 2010, MNRAS, 408, 2115
Mannucci F. et al., 2009, MNRAS, 398, 1915
Mannucci F., Salvaterra R., Campisi M. A., 2011, MNRAS, 414, 1263
Masters D. et al., 2014, ApJ, 785, 153
McCarthy I. G., Frenk C. S., Font A. S., Lacey C. G., Bower R. G., Mitchell N. L., Balogh M. L., Theuns T., 2008, MNRAS, 383, 593
McGaugh S. S., 1991, ApJ, 380, 140
McLean I. S. et al., 2012, in Society of Photo-Optical Instrumentation Engineers (SPIE) Conference Series, Vol. 8446, Society of Photo-Optical Instrumentation Engineers (SPIE) Conference Series
Mihos J. C., Hernquist L., 1996, ApJ, 464, 641
Nagao T., Maiolino R., Marconi A., 2006, A&A, 459, 85
Nagashima M., Lacey C. G., Baugh C. M., Frenk C. S., Cole S., 2005a, MNRAS, 358, 1247
Nagashima M., Lacey C. G., Okamoto T., Baugh C. M., Frenk C. S., Cole S., 2005b, MNRAS, 363, L31
Nakajima K., Ouchi M., 2014, MNRAS, 442, 900
Nakajima K., Ouchi M., Shimasaku K., Hashimoto T., Ono Y., Lee J. C., 2013, ApJ, 769, 3
Newman S. F. et al., 2014, ApJ, 781, 21
Newman S. F. et al., 2012, ApJ, 752, 111
Okamoto T., Nagashima M., 2003, ApJ, 587, 500
Oppenheimer B. D., Davé R., 2008, MNRAS, 387, 577
Peng Y.-j., Maiolino R., 2014, MNRAS, 438, 262
Pentericci L., Kurk J. D., Carilli C. L., Harris D. E., Miley G. K., Röttgering H. J. A., 2002, A&A, 396, 109
Pettini M., Pagel B. E. J., 2004, MNRAS, 348, L59
Prieto M. et al., 2013, MNRAS, 428, 999
Puech M., Flores H., Hammer F., Lehnert M. D., 2006, A&A, 455, 131
Salim S. et al., 2007, ApJS, 173, 267
Salpeter E. E., 1955, ApJ, 121, 161
Sanders R. L. et al., 2014, ArXiv e-prints
Shapley A. E., Coil A. L., Ma C.-P., Bundy K., 2005a, ApJ, 635, 1006
Shapley A. E. et al., 2014, ArXiv e-prints
Shapley A. E., Steidel C. C., Erb D. K., Reddy N. A., Adelberger K. L., Pettini M., Barmby P., Huang J., 2005b, ApJ, 626, 698
Shimakawa R. et al., 2014a, ArXiv e-prints
Shimakawa R., Kodama T., Tadaki K.-i., Tanaka I., Hayashi M., Koyama Y., 2014b, MNRAS, 441, L1
Shirazi M., Brinchmann J., Rahmati A., 2014, ApJ, 787, 120
Smail I. et al., 2014, ApJ, 782, 19
Springel V. et al., 2005, Nature, 435, 629
Steidel C. C., Erb D. K., Shapley A. E., Pettini M., Reddy N., Bogosavljević M., Rudie G. C., Rakic O., 2010, ApJ, 717, 289
Steidel C. C. et al., 2014, ArXiv e-prints
Steidel C. C., Shapley A. E., Pettini M., Adelberger K. L., Erb D. K., Reddy N. A., Hunt M. P., 2004, ApJ, 604, 534
Stott J. P. et al., 2013, MNRAS, 436, 1130
Suzuki R. et al., 2008, PASJ, 60, 1347
Tadaki K.-i. et al., 2014, ArXiv e-prints
Tadaki K.-i., Kodama T., Tanaka I., Hayashi M., Koyama Y., Shimakawa R., 2013, ApJ, 778, 114
Thomas D., Maraston C., Bender R., Mendes de Oliveira C., 2005, ApJ, 621, 673
Tremonti C. A. et al., 2004, ApJ, 613, 898
Troncoso P. et al., 2014, A&A, 563, A58
Valentino F. et al., 2014, ArXiv e-prints
Veilleux S., Osterbrock D. E., 1987, ApJS, 63, 295
Whitaker K. E., Rigby J. R., Brammer G. B., Gladders M. D., Sharon K., Teng S. H., Wuyts E., 2014, ArXiv e-prints
Whitaker K. E., van Dokkum P. G., Brammer G., Franx M., 2012, ApJ, 754, L29
Wuyts E., Rigby J. R., Gladders M. D., Sharon K., 2014, ApJ, 781, 61
Wuyts S. et al., 2013, ApJ, 779, 135
Yabe K., Ohta K., Akiyama M., Iwamuro F., Tamura N., Yuma S., Dalton G., Lewis I., 2014a, ArXiv e-prints
Yabe K. et al., 2014b, MNRAS, 437, 3647
Yabe K. et al., 2012, PASJ, 64, 60
Yoshikawa T. et al., 2010, ApJ, 718, 112
Zahid H. J., Dima G. I., Kudritzki R.-P., Kewley L. J., Geller M. J., Hwang H. S., Silverman J. D., Kashino D., 2014a, ApJ, 791, 130
Zahid H. J., Geller M. J., Kewley L. J., Hwang H. S., Fabricant D. G., Kurtz M. J., 2013, ApJ, 771, L19
Zahid H. J. et al., 2014b, ApJ, 792, 75

APPENDIX A: DUST EXTINCTION ACROSS THE MASS–METALLICITY RELATION IN SDSS GALAXIES

In order to discuss the effect of possible sampling bias on the derived gaseous metallicities between the UV-selected galaxies (which are strongly affected by dust extinction) and the Hα selected galaxies, we here investigate the correlation between the amount of dust extinction and the deviation from the M–Z relation in the SDSS SF galaxies.

For this purpose, we select Hα emitters in the SDSS in the same way as we use in this paper (see §2.1). Fig. A1a shows the M–Z relation of these galaxies obtained using the N2 index (Pettini & Pagel 2004). Fig. A1b represents the deviations in metallicity from the M–Z relation as a function of dust obscuration in Hα line. We divide the sample into 11 bins according to their stellar masses (Fig. A1a), and plot the locus of median values of Δ log (O/H) as a function of $A_{H\alpha}$ for each mass bin in a different colour (Fig. A1b). As a result, we do not find any strong correlation between these two quantities, meaning that the effect of dust obscuration in the UV selected sample does not introduce any significant bias to the derived metallicities. Therefore we conclude that the selection effect we discuss in §4.2 should be minimal.

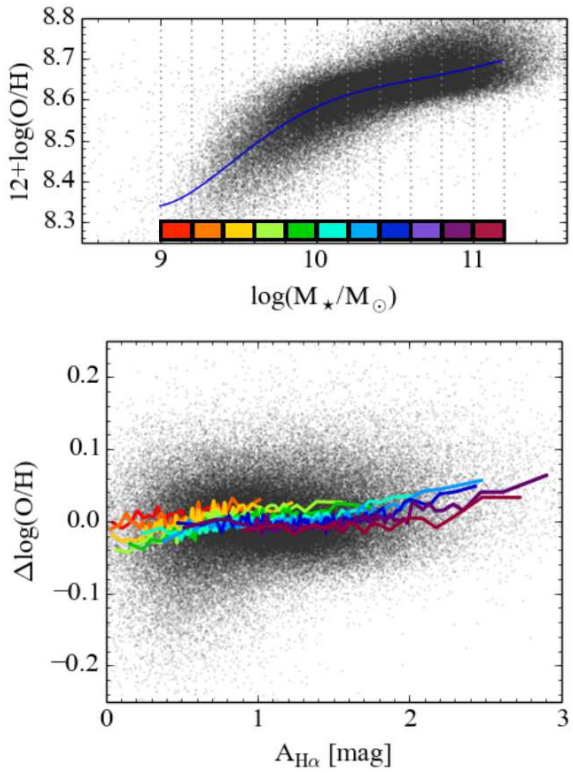

Figure A1. (a) The upper panel shows the mass–metallicity relation of SDSS galaxies based on the N2 index (Pettini & Pagel 2004). (b) The lower panel represents the offset of the metallicity (Δ log (O/H)) from the median locus of the M–Z relation shown in the upper panel (blue curve) as a function of $A_{H\alpha}$ derived from the Balmer decrement. Colour-coded lines indicate median values of Δlog(O/H) as a function of $A_{H\alpha}$ for the subsamples divided according to their stellar masses as shown in the vertical dotted lines in the upper panel and the corresponding colour coding.